Accepted Manuscript

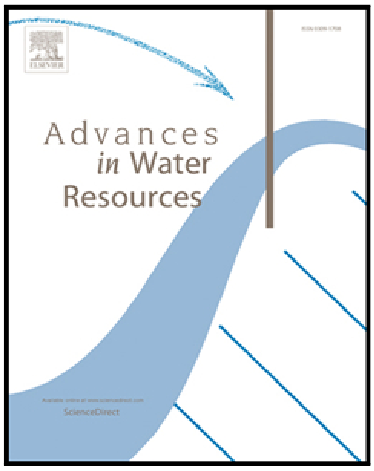

River banks and channel axis curvature: effects on the longitudinal dispersion in alluvial rivers

Stefano Lanzoni, Amena Ferdousi, Nicoletta Tambroni

PII: S0309-1708(17)30748-0
DOI: 10.1016/j.advwatres.2017.10.033
Reference: ADWR 2997

To appear in: *Advances in Water Resources*

Received date: 26 July 2017
Revised date: 27 October 2017
Accepted date: 28 October 2017

Please cite this article as: Stefano Lanzoni, Amena Ferdousi, Nicoletta Tambroni, River banks and channel axis curvature: effects on the longitudinal dispersion in alluvial rivers, *Advances in Water Resources* (2017), doi: 10.1016/j.advwatres.2017.10.033

River banks and channel axis curvature: effects on the longitudinal dispersion in alluvial rivers

Stefano Lanzoni[a], Amena Ferdousi[a], Nicoletta Tambroni[b]

[a] *Department of Civil, Environmental and Architectural Engineering, University of Padua, Italy*
[b] *Department of Civil, Chemical and Environmental Engineering, University of Genova, Genova, Italy*

Abstract

The fate and transport of soluble contaminants released in natural streams are strongly dependent on the spatial variations of the flow field and of the bed topography. These variations are essentially related to the presence of the channel banks and the planform configuration of the channel. Large velocity gradients arise near to the channel banks, where the flow depth decreases to zero. Moreover, single thread alluvial rivers are seldom straight, and usually exhibit meandering planforms and a bed topography that deviates from the plane configuration. Channel axis curvature and movable bed deformations drive secondary helical currents which enhance both cross sectional velocity gradients and transverse mixing, thus crucially influencing longitudinal dispersion. The present contribution sets up a rational framework which, assuming mild sloping banks and taking advantage of the weakly meandering character often exhibited by natural streams, leads to an analytical estimate of the contribution to longitudinal dispersion associated with spatial non-uniformities of the flow field. The resulting relationship stands from a physics-based modeling of the behaviour of natural rivers, and expresses the bend averaged longitudinal dispersion coefficient as a function of the relevant hydraulic and morphologic parameters. The

*Corresponding author
Email addresses: stefano.lanzoni@unipd.it (Stefano Lanzoni), a_ferdousi@easternuni.edu.bd (Amena Ferdousi), stefano.lanzoni@unipd.it (Nicoletta Tambroni)

treatment of the problem is river specific, since it relies on a explicit spatial description, although linearized, of flow field that establishes in the investigated river. Comparison with field data available from tracer tests supports the robustness of the proposed framework, given also the complexity of the processes that affect dispersion dynamics in real streams.

Keywords: Alluvial rivers, Dispersion, meandering rivers

---

1. Introduction

Estimating the ability of a stream to dilute soluble pollutants is a fundamental issue for the efficient management of riverine environments. Rapidly varying inputs of contaminants, such as those associated with accidental spills of toxic chemicals and intermittent discharge from combined sewer overflows, as well as temperature variations produced by thermal outflows, generate a cloud that spreads longitudinally affecting the fate of the pollutant.

The classical treatment of longitudinal transport in turbulent flows relies on the study put forward by *Taylor* (1954) for pipe flows, and extended to natural channels by *Fischer* (1967). Taylor's analysis indicates that, far enough from the source (in the so called equilibrium region), the cross-sectionally averaged tracer concentration, C, satisfies a one-dimensional advection-diffusion equation, embodying a balance between lateral mixing and nonuniform shear flow advection (Fickian dispersion model). Under the hypothesis that the velocity field is statistically steady and the investigated channel reach is geometrically homogeneous and extends far inside the equilibrium region, the advection-diffusion equation prescribes that the variance of C in the along stream direction s^* increases linearly with time and any skewness, introduced by velocity shear close to the contaminant source (i.e., in the advective zone) or by the initial distribution of contaminant, begins to slowly decay, eventually leading at any instant to a Gaussian distribution of $C(s^*)$ (*Chatwin and Allen*, 1985). The coefficient of apparent diffusivity K^* governing this behavior, usually denoted as dispersion coefficient, is much greater than the coefficient for longitudinal diffusion by turbulence alone.

Many engineering and environmental problems concerning the fate and transport of pollutants and nutrients are tackled resorting to the one-dimensional advection-diffusion approach (*Rinaldo et al.*, 1991; *Wallis*, 1994; *Schnoor*, 1996; *Revelli and Ridolfi*, 2002; *Botter and Rinaldo*, 2003) and, therefore, require a suitable specification of the longitudinal dispersion coefficient K^*. Also within the context of much more refined models developed to account for the formation of steep concentration fronts and elongated tails caused by storage and delayed release of pollutant in dead zones (see, among many others, *Czernuszenko et al.* (1998), *Bencala and Walters* (1983) and *Bear and Young* (1983)), a reliable estimate of longitudinal dispersion in the main stream (quantified by K^*) is fundamental to properly account for chemical and biological processes acting in different channel regions (*Lees et al.*, 2000).

Several procedures have so far been proposed to estimate the longitudinal dispersion coefficient from either tracer data (*Rutherford*, 1994) or velocity measurements at a number of cross sections (*Fischer*, 1967). These approaches are usually expensive and time consuming. The lack of experimental data which characterizes many applications, as well as the necessity of specifying K^* when carrying out preliminary calculations, has thus stimulated the derivation of various semi-empirical and empirical relationships (*Fischer*, 1967; *Liu*, 1977; *Iwasa and Aya*, 1991; *Seo and Cheong*, 1998; *Deng et al.*, 2001; *Kashefipour and Falconer*, 2002; *Deng et al.*, 2002; *Shucksmith et al.*, 2011; *Sahay and Dutta*, 2009; *Etamad-Shahidi and Taghipour*, 2012; *Li et al.*, 2013; *Zeng and Huai*, 2014; *Disley et al.*, 2015; *Sattar and Gharabaghi*, 2015; *Noori et al.*, 2017; *Wang and Huai*, 2016), which can be cast in the general form:

$$K^* = \kappa_0 \frac{\beta^{\,\kappa_1}}{(\sqrt{c_{fu}})^{\,\kappa_2}}\, B^*\, U_u^*, \tag{1}$$

where β is the ratio of half channel with, B^*, to mean flow depth, D_u^*, c_{fu} is the friction coefficient, U_u^* is the mean value of the cross-sectionally averaged flow velocity within the reach of interest and κ_i ($i = 0, 1, 4$) are suitable constants, specified in Table 1. Note that in Table 1 we have just reported the main formulas, for sake of completeness a wider list of relationships is given in the Supplementary Information.

Table 1: Values attained by the constants of the generalized formula (1) and by the associated mean value of the discrepancy ratio d_r (defined in Section 4.2) for various predictors available in literature, namely: (1) *Fischer et al.* (1979); (2) *Seo and Cheong* (1998); (3) *Liu* (1977); (4) *Kashefipour and Falconer* (2002); (5) *Iwasa and Aya* (1991); (6) *Deng et al.* (2001); (7) *Wang and Huai* (2016). The dimensionless transverse eddy diffusivity, e_t, and mixing coefficient, k_t, are defined in Section 2.

	(1)	(2)	(3)	(4)	(5)	(6)	(7)
κ_0	0.044	9.1	0.72	10.612	5.66	$0.06/(e_t+k_t)$	22.7
κ_1	1.0	-0.38	1.0	-1.0	0.5	0.67	-0.64
κ_2	1.0	0.428	-0.5	1.0	-1.0	1.0	0.16
$< d_r >$	1.05	1.24	1.10	1.05	1.04	0.63	1.13

The empirical parameters that are introduced in these relations to address the complexity embedded in the mixing process still make the quantifying of K^* a challenging task. In many cases, the proposed predictor provides only a rough estimate, and the discrepancy between the predicted values of K^* and those determined from tracer test is quite high. Among the many reasons responsible for this high scatter, one may be the prismatic character assumed as the basis of the Fickian solution (*Wang and Huai*, 2016). Nevertheless, natural channels are usually characterized by a complex bed topography, which strongly affects the flow field and, hence, the longitudinal dispersion (*Guymer*, 1998), but is only roughly accounted for in the various approaches. In addition, in some cases a suitable tuning of the empirical parameters is needed in order to achieve a good agreement with the experimental data (*Deng et al.*, 2001).

Many of the existing expressions for predicting the longitudinal dispersion in rivers have been developed by minimizing the error between predicted and measured (through tracer tests) dispersion coefficients. These relations generally differ in terms of the relevant dimensionless groups (determined through dimensional analysis) and of the optimization technique (e.g., nonlinear multi regression, genetic and population-based evolutionary algorithms) used to calibrate the coefficients of the predictor (*Seo and Cheong* (1998); *Kashefipour and Falconer* (2002); *Sahay and Dutta* (2009); *Disley et al.* (2015); *Noori et al.* (2017)). More recently, the dataset provided by the dispersion coefficients measured in the field has been used for training and testing artificial neural networks or bayesan networks (*Alizadeh et al.*, 2017). A less few attempts were devoted to derive analytical relationships by substituting in the triple integral ensuing from Fischer analysis of shear flow dispersion the flow field that, under the uniform-flow assumption, establishes in stable straight channels (*Deng et al.*, 2001) and in meandering rivers (*Deng et al.*, 2002). In the present contribution we follow this latter approach, which has the advantage of being river specific, i.e., to relate the dispersion coefficient to the shear flow dispersion that actually takes place in the river under investigation. The improvement with respect to the contributions by *Deng et al.* (2001, 2002) are essentially related to the morphodynamics-based modelling of the flow that establishes in alluvial rivers. In the case of straight rivers, rather than using the general hydraulic geometry relationship for stable cross sections, we propose a specific treatment of the shear flow effects by dividing the cross section into a central flat-bed region and two gently sloping banks computing the flow field therein. In the case of meandering rivers, the flow field outside the boundary layers that form near to the banks is solved explicitly, although in a linearised way, accounting parametrically for the secondary flow circulations induced by streamline curvatures and computing the bed topography by solving the two-dimensional sediment balance equation.

The aim of the present contribution is thus to develop physics-based, analytic predictions of the longitudinal dispersion coefficient, accounting for the cross-sectional morphology occurring in alluvial rivers. More specifically, we intend to relate the estimates of K^* to the relevant hydraulic, geometric and sedimentologic parameters (flow discharge, bed slope, representative sediment size, bank geometry) governing the steady flow in an alluvial river. First, we apply to the flow field which establishes in sinuous, movable bed channels the perturbative procedure developed by *Smith* (1983), that accounts for the fast variations of concentration induced across the section by irregularities in channel geometry and the presence of bends. This methodology, introducing a reference system moving downstream with the contaminant cloud and using a multiple scale perturbation technique, allows the derivation of a dispersion equation relating entirely to shear flow dispersion the along channel changes in the cross-sectionally averaged concentration. Next, we take advantage of the weakly meandering character of many natural rivers to clearly separate the contributions to longitudinal dispersion provided by the various sources of nonuniformities. At the leading order of approximation, corresponding to the case of a straight channel, we consider the differential advection related to the presence of channel banks, solving the flow field by means of a rational perturbation scheme (*Tubino and Colombini*, 1992). At the first order of approximation, we introduce the correction to K^* due to the presence of bends by using the hydro-morphodynamic model of *Frascati and Lanzoni* (2013).

The proposed methodology is finally validated through the comparison with the tracer test data collected in almost straight and in meandering rivers. Among others, we consider the detailed dataset provided by *Godfrey and Frederick* (1970), which includes detailed measurements of flow depth, longitudinal velocity, and the temporal evolution of the tracer concentration at different cross sections, as well as estimates of K^* based on the method of moments. These concentration data are here reanalyzed by considering the Chatwin's method (*Chatwin*, 1980), which indicates if and where a Fickian model likely applies, and the routing method, based on the Hayami solution (*Rutherford*, 1994). We anticipate that the proposed framework provides estimates of K^* that are in reasonable good agreement with the values computed from tracer tests.

The paper is organized as follows. The mathematical problem is formulated in Section 2, with particular emphasis on the typical temporal and spatial scales which allow to set up a rational perturbative framework and eventually determine the overall structure of the dispersion coefficient in alluvial channels. The analytical solutions of the depth averaged flow field used to compute K^* are described in Section 3. The comparison with available field data is reported in Section 4, while Section 5 is devoted to the discussion of the results. Finally, Section 6 summarizes the concluding remarks.

2. Formulation of the problem

We consider the behavior of a passive, non-reactive contaminant which (e.g., due to an accidental spill) is suddenly released in an alluvial channel with a compact cross section and, in general, a meandering planform. The river cross section bed is assumed to vary slowly in the transverse direction as the banks are approached. This assumption allows for solving the flow field by adopting a closure model of turbulence in which the turbulent viscosity ν_T^* is a function of the local flow condition (see Section 3.1). The channel has fixed banks, a constant free surface width $2B^*$, a longitudinal mean slope S, and conveys a constant discharge Q^* (hereafter a star superscript will be used to denote dimensional variables). The reach averaged value of the flow depth is D_u^*. The corresponding cross-section area is $A_u^* = 2B^* D_u^*$, while the cross-sectionally averaged mean velocity is $U_u^* = Q^*/A_u^*$. The erodible channel bed is assumed to be made up of a uniform cohesionless sediment with grain size d_{gr}^*, density ρ_s, and immersed relative density $\Delta = (\rho_s - \rho)/\rho$, with ρ the water density. Moreover, we denote by $\beta = B^*/D_u^*$ the half width to depth ratio, $u_{fu}^* = (gD_u^* S)^{1/2}$ the friction velocity (with g the gravitational constant), and $c_{fu} = (u_{fu}^*/U_u^*)^2$ the friction coefficient. These two latter quantities are influenced by the bed configuration, which can be either plane or covered by bedforms such as ripples and dunes, depending on the dimensionless grain size $d_{gr} = d_{gr}^*/D_u^*$, and the Shields parameter, $\tau_{*u} = u_{fu}^{*2}/(\Delta g d_{gr}^*)$.

2.1. The 2-D dimensionless advection-diffusion equation

The problem can be conveniently studied introducing the curvilinear orthogonal coordinate system (s^*, n^*, z^*) shown in Figure 1a, where s^* is the longitudinal curvilinear coordinate coinciding with the channel axis, n^* is the horizontal coordinate normal to s^*, and z^* is the upward directed axis. The two-dimensional advection-diffusion equation for the depth-averaged concentration $c(s^*, n^*, t^*)$ reads (*Yotsukura*, 1977):

$$\begin{aligned} h_s D^* \frac{\partial c}{\partial t^*} \quad &+ \quad D^* U^* \frac{\partial c}{\partial s^*} + h_s\, D^* V^* \frac{\partial c}{\partial n^*} \\ &= \quad \frac{\partial}{\partial s^*}(k_s^* \, \frac{D^*}{h_s} \, \frac{\partial c}{\partial s^*}) + \frac{\partial}{\partial n^*}(k_n^* \, h_s \, D^* \, \frac{\partial c}{\partial n^*}) \end{aligned} \tag{2}$$

where t^* denotes time, D^* is the local flow depth, U^* and V^* are the depth-averaged longitudinal and transverse components of the velocity, and k_s^* and k_n^* are longitudinal and transverse mixing coefficients which account for the combined effect of vertical variations of velocity and turbulent diffusion. Moreover, h_s is a metric coefficient, arising from the curvilinear character of the longitudinal coordinate, defined as:

$$h_s = 1 + \frac{n^*}{r^*} = 1 + \nu\, n\, \mathcal{C}, \tag{3}$$

where $r^*(s^*)$ is the local radius of curvature of the channel axis, assumed to be positive when the center of curvature lies along the negative n^*-axis, $\nu = B^*/R_0^*$ is the curvature ratio, $n = n^*/B^*$ is the dimensionless transverse coordinate, $\mathcal{C} = R_0^*/r^*$ is the dimensionless channel curvature, and R_0^* is twice the minimum value of r^* within the meandering reach.

In meandering channels the cross-sectionally averaged concentration undergoes relatively small and rapidly changing gradients, associated with the spatial variations of the flow field along the bends, and a slower evolution due to longitudinal dispersion. In order to deal with the fast concentration changes acting at the meander scale, it proves convenient to introduce a pseudo-lagrangian, volume following coordinate, ξ^*, which travels downstream with the contaminant cloud and accounts for the fact that the cross-sectionally averaged velocity Q^*/A^* in not constant along the channel (*Smith*, 1983). This coordinate is defined as:

$$\xi^* = \frac{1}{A_u^*} \int_0^{s^*} \mathcal{A}^* \, ds^* - U_u^* \, t^* \tag{4}$$

where the integral on the right side is the water volume from the origin of the coordinate system to the generic coordinate s^*, while

$$A^* = \int_{-B^*}^{B^*} D^* \, dn^*, \qquad \mathcal{A}^* = \int_{-B^*}^{B^*} h_s D^* \, dn^*. \tag{5}$$

Clearly, $\mathcal{A}^*$ and A^* can vary along s^* as a consequence of the variations of section geometry induced by the bed topography that establishes in the meandering channel. The derivation chain rule implies that:

$$\frac{\partial}{\partial s^*} = \frac{\partial}{\partial s^*} + \mathcal{A} \, \frac{\partial}{\partial \xi^*}, \qquad \frac{\partial}{\partial t^*} = \frac{\partial}{\partial t^*} - U_u^* \, \frac{\partial}{\partial \xi^*} \tag{6}$$

where $\mathcal{A} = \mathcal{A}^*/A_u^*$. Consequently, for an observer moving with velocity U_u^* (i.e., with the advected pollutant cloud) the dilution of the concentration associated with longitudinal dispersion is accounted for by the coordinate ξ^* and occurs at a length scale comparable with the length of the contaminant cloud, L_c^*. It then results that $c = c(s^*, n^*, \xi^*, t^*)$, and equation (2) can be rewritten as:

$$D^* U^* \frac{\partial c}{\partial s^*} + h_s \, D^* V^* \frac{\partial c}{\partial n^*} - \frac{\partial}{\partial n^*}(k_n^* \, h_s \, D^* \frac{\partial c}{\partial n^*}) = D^* \left(h_s \, U_u^* - \mathcal{A} U^* \right) \frac{\partial c}{\partial \xi^*} - h_s D^* \frac{\partial c}{\partial t^*} +$$
$$+ \frac{\partial}{\partial s^*} \left(k_s^* \frac{D^*}{h_s} \frac{\partial c}{\partial s^*} + \mathcal{A} \, k_s^* \frac{D^*}{h_s} \frac{\partial c}{\partial \xi^*} \right) + \mathcal{A} \frac{\partial}{\partial \xi^*} \left(k_s^* \frac{D^*}{h_s} \frac{\partial c}{\partial s^*} + \mathcal{A} \, k_s^* \frac{D^*}{h_s} \frac{\partial c}{\partial \xi^*} \right) \tag{7}$$

In order to better appreciate how transverse mixing, differential advection, longitudinal dispersion and spatial changes in bed topography contribute to dilute the pollutant concentration, equation (2) is made dimensionless introducing the following scaling:

$$s^* = L^* \, s, \qquad \xi^* = L_c^* \, \xi, \qquad n^* = B^* \, n, \qquad D^* = D_u^* \, D, \tag{8}$$

$$t^* = T_0^*\, t \qquad (U^*, V^*) = U_u^*\,(U, \frac{L^*}{B^*}\, V), \qquad (k_s^*, k_n^*) = k_{nu}^*(k_s, k_n) \tag{9}$$

where L^* is the average intrinsic meander length within the investigated reach (see Figure 1a), k_{nu}^* is the transverse mixing coefficient for a straight channel configuration, and T_0^* is the typical timescale at which longitudinal dispersion operates within the contaminant cloud.

Besides the timescale $T_0^* = L_c^{*\,2}/K_u^*$ (where K_u^* is a typical dispersion coefficient), other two timescales, $T_1^* = L_c^*/U_u^*$ and $T_2^* = B^{*\,2}/k_{nu}^*$, characterize the processes (longitudinal dispersion, differential advection and transverse mixing) that govern the concentration dynamics of the pollutant cloud. In order to ensure that they are well separated (*Fischer*, 1967; *Smith*, 1983), we introduce the small parameter

$$\epsilon = \frac{k_{nu}^*}{B^* U_u^*}, \tag{10}$$

and recall the relationships usually adopted to predict the transverse mixing coefficients k_{nu}^* and K_u^*.

The rate of transverse mixing is determined by turbulent diffusion, quantified by the depth averaged transverse eddy diffusivity e_t^*, and vertical variations in the transverse velocity, quantified by the transverse dispersion coefficient k_t^* (*Rutherford*, 1994). Both coefficients scale as $u_{fu}^* D_u^*$ and, consequently, the transverse mixing coefficient can be expressed as:

$$k_{nu}^* = (e_t + k_t)\, u_{fu}^*\, D_u^* \tag{11}$$

Recalling that $u_{fu}^*\, D_u^* = B^*\, U_u^*\, \sqrt{c_{fu}}/\beta$, it results that $\epsilon = (e_t + k_t)\, \sqrt{c_{fu}}/\beta$. Experimental observations in straight rectangular flumes indicate that e_t usually falls in the range (0.10 - 0.26), with a mean value equal to 0.15 (*Rutherford*, 1994). On the other hand, for large rivers the transverse dispersion coefficient k_t has been related to the mean flow velocity and the channel width through a relation of the form (*Smeithlov*, 1990):

$$k_t = \left[\frac{1}{3520} \Big(\frac{U_u^*}{u_{fu}^*} \Big) \Big(\frac{2B^*}{D_u^*} \Big)^{1.38} \right] \tag{12}$$

Observing that the ratio $\sqrt{c_{fu}}/\beta$ attains values of order $O(10^{-2})$ and $O(10^{-3})$ in gravel and sandy rivers (*Hey and Throne*, 1986; *Parker*, 2004), it results that the parameter ϵ is indeed small.

According to the semi-empirical relationship developed by *Fischer et al.* (1979), $K_u^* = 0.044\,(B^* U_u^*)^2/(u_{fu}^* D_u^*)$. This functional dependence is confirmed by the dispersion data reported by *Rutherford* (1994), indicating that the dimensionless ratio $K_u^*/B^* U_u^*$ mostly falls in the range $0.14 - 36$, with mean 4.4 and standard deviation 5.0. We can then write:

$$\frac{k_{nu}^*}{K_u^*} = \frac{k_n + k_t}{0.044} \frac{c_{fu}}{\beta^2} \sim \epsilon^2, \tag{13}$$

Consequently, $T_1^*/T_0^* = \epsilon$ and $T_2^*/T_0^* = \epsilon^2$, provided that $B^*/L_c^* = \epsilon^2$, that is the contaminant cloud has reached a length of order of hundred of meters or kilometers, depending on the width of the channel section. This result implies that the three time scales are well separated, i.e. $T_0^* < T_1^* < T_2^*$. In other words, the longitudinal dispersion operates on a timescale much slower than the timescale characterizing transverse mixing which, in turn is much faster than nonuniform advection (*Fischer*, 1967; *Smith*, 1983).

The derivation of the longitudinal dispersion coefficient takes advantage of the small character of the parameter ϵ, ensuring the separation of the three timescales. Substituting the dimensionless variables (8) and (9) into equation (7), we obtain:

$$\begin{aligned} \mathcal{L}c &= \epsilon\, D \big(h_s - \mathcal{A} U\big) \frac{\partial c}{\partial \xi} - \epsilon^2\, h_s\, D \frac{\partial c}{\partial t} \\ &+ \epsilon^2 \Big(\gamma \frac{\partial}{\partial s} + \epsilon \mathcal{A} \frac{\partial}{\partial \xi} \Big) \Big(\frac{\gamma}{\epsilon}\, k_s\, \frac{D}{h_s} \frac{\partial c}{\partial s} + \mathcal{A}\, k_s\, \frac{D}{h_s} \frac{\partial c}{\partial \xi} \Big) \end{aligned} \tag{14}$$

where the differential operator $\mathcal{L}$ reads:

$$\mathcal{L} = \gamma\, D\,\big(U\frac{\partial}{\partial s} + h_s\, V\frac{\partial}{\partial n}\big) - \frac{\partial}{\partial n}\big(h_s\, D\, k_n \frac{\partial}{\partial n}\big) \tag{15}$$

The additional parameter $\gamma = \epsilon L_c^*/L^*$ arises because of the presence of two spatial scales. The spatial variations of c associated with longitudinal dispersion at the scale of the contaminant cloud are described by the slow variable ξ, whereas the comparatively small and rapidly changing variations in concentration across the flow associated with stream meandering are accounted for through the fast variables s, n. The parameter γ describes the relative importance of transverse mixing, which tends to homogenize the contaminant concentration, and nonuniform transport at the bend scale, which, on the contrary, enhances concentration gradients. It is readily observed that $\gamma = \epsilon^{-1}\lambda/2\pi$, where the dimensionless meander wavenumber $\lambda = 2\pi B^*/L^*$ typically ranges between 0.1 and 0.3 (*Leopold et al.*, 1964). The product $\gamma\epsilon$ then turns out of order $O(10^{-2})$ and, hence, gives rise to higher order terms in the perturbation analysis described in the next Section.

2.2. The longitudinal dispersion coefficient

The presence of different spatial and temporal scales can be handled employing a multiple scale technique (*Nayfeh*, 1973). To this purpose we expand the concentration $c = c(s, n, \xi, t)$ as:

$$c = c_0 + \epsilon\, c_1 + \epsilon^2\, c_2 + \dots \tag{16}$$

We substitute this expansion into (14), and consider the problems arising at various orders of approximation:

$$O(\epsilon^0) \quad \mathcal{L}\, c_0 = 0 \tag{17}$$

$$O(\epsilon) \quad \mathcal{L}\, c_1 = D\Big(h_s - U\mathcal{A}\Big)\frac{\partial c_0}{\partial \xi} \tag{18}$$

$$O(\epsilon^2) \quad \mathcal{L}\, c_2 = D\Big(h_s - U\mathcal{A}\Big)\,\frac{\partial c_1}{\partial \xi} - h_s D\,\frac{\partial c_0}{\partial t}, \tag{19}$$

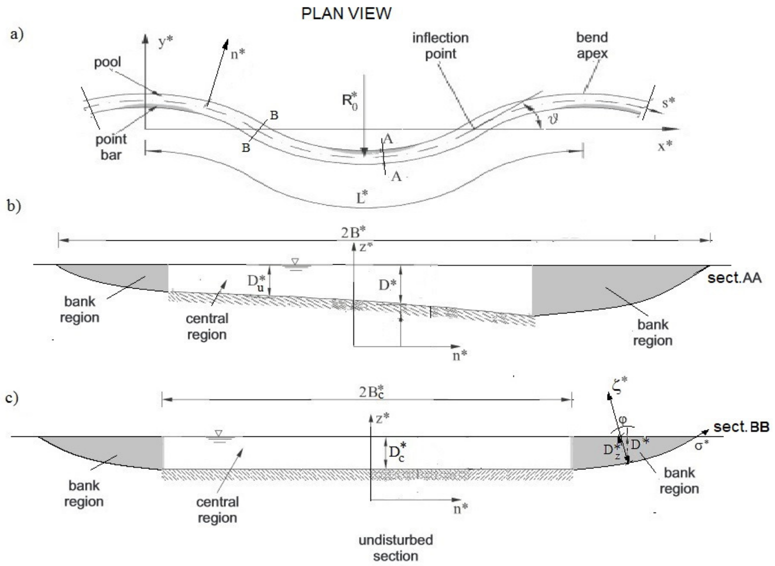

Figure 1: Sketch of a meandering channel and notations. a) Plan view. b) Typical cross-section in a neighborhood of the bend apex. Note the scour at the outer bank and the deposition caused by the point bar at the inner bank. c) Average cross-section, typically occurring nearby the inflection point of the channel axis.

coupled with the requirements that $\partial c_i/\partial n = 0$ ($i = 0$, 1, 2) at the channel banks, where the normal component of the contaminant flux vanishes.

The partial differential equations (17), (18) and (19) provide a clear insight into the structure of the contaminant concentration. Recalling that, for a steady open channel flow, the depth-averaged (i.e., two-dimensional) continuity equation, written in dimensionless form, reads:

$$\frac{\partial(UD)}{\partial s} + \frac{\partial(h_s V D)}{\partial n} = 0, \tag{20}$$

we integrate (17) across the section and find that c_0 does not depend on s, n and, hence, it is not affected by the fluctuations induced by flow meandering. Equation (18) suggests a solution of the form $c_1 = g_1(s,n)\,\partial c_0/\partial \xi$, with g_1 a function describing the nonuniform distribution across the section of the contaminant concentration. Similarly, equation (19) indicates that $c_2 = g_2(s,n)\,\partial^2 c_0/\partial\xi^2$. The depth-averaged concentration then results:

$$
\begin{aligned}
c(s,n,\xi,t) &= c_0(\xi,t) + \epsilon\, g_1(s,n)\,\frac{\partial c_0}{\partial \xi} \\
&+ \epsilon^2\, g_2(s,n)\,\frac{\partial^2 c_0}{\partial \xi^2} + O(\epsilon^3)
\end{aligned} \tag{21}
$$

and clearly discriminates the slower evolution due to longitudinal dispersion, embodied by the terms c_0, $\partial c_0/\partial\xi$, $\partial^2 c_0/\partial\xi^2$, from the small and rapidly varying changes associated with the spatial variations of the flow field, described by the functions g_1 and g_2.

Integrating (21) across the section and along a meander, the cross-sectionally averaged concentration can be approximated as $\bar{c} = c_0 + O(\epsilon^3)$ provided that $< \bar{g}_i >= 0$ $(i = 1, 2)$, where:

$$
\bar{c} = \frac{1}{2\mathcal{A}}\int_{-1}^{1} h_s D\, c\, dn, \quad \bar{g}_i = \frac{1}{2\mathcal{A}}\int_{-1}^{1} h_s D\, g_i\, dn, \quad \langle \bar{g}_i \rangle = \int_{s-1/2}^{s+1/2} \bar{g}_i\, ds \tag{22}
$$

It is important to note that only averaging (21) along the entire meander length ensures that the arbitrary constant embedded in g_i does not actually depend on s.

We are now ready to derive the advection-diffusion equation, governing the evolution of the cross-sectionally averaged concentration $\bar{c}$, and the related longitudinal dispersion coefficient. We sum together equations (18) and (19), integrated across the section and along a bend, and require that the flux of contaminant vanishes, i.e., $\int_{-1}^{1} DU g_i dn = 0$ (i =1,2), a condition needed in order to eliminate secular terms which would lead c_2 to grow systematically with s. We eventually obtain:

$$
\frac{\partial c_0}{\partial t} = K\,\frac{\partial^2 c_0}{\partial \xi^2} + O(\epsilon) \tag{23}
$$

where:

$$K = \langle \mathcal{A}^2 \mathcal{K} \rangle, \qquad \mathcal{K} = \frac{1}{2\,\mathcal{A}} \int_{-1}^{1} D\,(\frac{h_s}{\mathcal{A}} - U)\, g_1\, dn, \tag{24}$$

while the function $g_1(s,n)$, describing the cross-sectional distribution of the concentration, results from the solution of the $O(\epsilon)$ equation:

$$\mathcal{L}\, g_1 = D\,(h_s - U\mathcal{A}), \tag{25}$$

with the requirements that $\partial g_1/\partial n = 0$ at the channel banks, where the normal component of the contaminant flux vanishes, and $\langle \bar{g}_1 \rangle = 0$.

Before proceeding further, some observations on the expression (24) are worthwhile. In accordance with *Fischer* (1967), the contribution to longitudinal dispersion provided by vertical variations of the velocity profile (embodied by the terms of (14) containing k_s) is of minor importance. Longitudinal dispersion is essentially governed by shear flow dispersion induced by the nonuniform distribution across the section of both the contaminant concentration, accounted for through the function $g_1(s,n)$, and the flow field, quantified by $D\,(h_s - U\mathcal{A})$. This latter term, however, differs from the much simpler term $(1-U)$ that would arise in the classical treatment pursued by *Fischer* (1967), as a consequence of the fact that here the mean flow velocity can in general vary along the channel, as accounted for through the volume-following coordinate ξ. In addition, it is important to observe that the bend averaged coefficient K is always positive while, in the presence of river reaches characterized by rapid longitudinal variations of the flow field, the coefficient $\mathcal{K}$ can also attain negative values, thus favoring spurious instabilities (*Smith*, 1983).

Finally, it is useful to relate the local and the bend averaged dispersion coefficients, K and $\mathcal{K}$, to the local dispersion coefficient $\mathcal{D}$ that arises when considering only the fast coordinate s. Decomposing the concentration c and velocity U^* as the sum of their cross-sectionally averaged values, $\bar{c}$, $\bar{U}^*$, plus the corresponding fluctuations c', U'^*, the classical one-dimensional advection-dispersion equation results:

$$\frac{\partial \bar{c}}{\partial t^*} + \frac{Q^*}{\mathcal{A}^*}\frac{\partial \bar{c}}{\partial s^*} = -\frac{1}{\mathcal{A}}\frac{\partial}{\partial s^*}\int_{-B^*}^{B^*} D^* {U'}^* c' dn^* \tag{26}$$

Setting $c' = (B^{*2} U_u^* / k_{nu}^*)\, g_1\, \partial \bar{c}/\partial s^*$, after some algebra it can be demonstrated that:

$$\mathcal{D}^* = \frac{(U_u^*\, B^*)^2}{k_{nu}^*}\,\mathcal{D}, \qquad \mathcal{D} = \frac{1}{2\,\mathcal{A}}\int_{-1}^{1} D\,(\bar{U} - U)\, g_1\, dn, \tag{27}$$

and, consequently, $\mathcal{K} = \mathcal{D}$ and $K = \langle \mathcal{A}^2 \mathcal{D} \rangle$.

2.3. Structure of the longitudinal dispersion coefficient in meandering channels

Natural channels are seldom straight. In the general case of a meandering planform configuration, the problem can be faced by taking advantage of the fact that, in nature, the curvature ratio ν appearing in (3) is typically a small parameter, ranging in the interval $0.1 - 0.2$ (*Leopold et al.*, 1964). This evidence is widely used to describe the flow field in meandering channels (*Seminara*, 2006) and to model their long term evolution (*Frascati and Lanzoni*, 2010, 2013). It implies that the flow field and the bed topography of a meandering channel can be determined by studying the relatively small perturbations associated with deviations from a straight channel configuration. We then introduce the expansions:

$$\begin{aligned}[U(s,n),\, D(s,n),\, \mathcal{A}(s)] = [U_0(n),\, D_0(n),\, 1] + \nu\, [U_1(s,n),\, D_1(s,n),\, \mathcal{A}_1(s)] \\ + \nu^2\, [U_2(s,n),\, D_2(s,n),\, \mathcal{A}_2(s)] + O(\nu^3)\end{aligned} \tag{28}$$

where the unperturbed $O(\nu^0)$ state corresponds to a straight channel. Similarly, we expand in terms of ν the function g_1 and the dimensionless transverse mixing coefficient k_n:

$$[k_n(s,n), g_1(s,n)] = [k_{n0}(n),\, g_{10}(n)] + \nu\, [k_{n1}(s,n),\, g_{11}(s,n)] + O(\nu^2) \tag{29}$$

The longitudinal dispersion coefficient in meandering channels is determined by substituting (28) and (29) into (24), and recalling (3). We obtain:

$$K = K_0 + \nu\, K_1 + \nu^2\, K_2\, +\, O(\nu^3) \tag{30}$$

where

$$K_0 = \frac{1}{2}\int_{-1}^{1} (1 - U_0)\, D_0\, g_{10}\, dn \tag{31}$$

$$\begin{aligned} K_1 = & \frac{1}{2}\int_{-1}^{1} (1 - U_0) < D_0 g_{11} + D_1\, g_{10} > \, dn\, + \\ & + \frac{1}{2}\int_{-1}^{1} < n\mathcal{C} - U_1 - U_0\mathcal{A}_1 > \, D_0\, g_{10}\, dn \end{aligned} \tag{32}$$

$$\begin{aligned} K_2 = & \frac{1}{2}\int_{-1}^{1} (1 - U_0) < D_0\, g_{12} + D_1\, g_{11} + D_2\, g_{10} > \, dn\, + \\ & + \frac{1}{2}\int_{-1}^{1} < (n\mathcal{C} - U_1 - U_0\mathcal{A}_1)\, (D_0\, g_{11} + D_1\, g_{10}) > \, dn\, + \\ & - \frac{1}{2}\int_{-1}^{1} < U_2 + U_1\mathcal{A}_1 + U_0\mathcal{A}_2 > \, D_0\, g_{10}\, dn \end{aligned} \tag{33}$$

It is immediately recognized that the leading order contribution K_0 corresponds to the classical solution obtained by *Fischer* (1967). It accounts for dispersion effects which arise in a straight uniform flow as a consequence of the transverse gradients experienced by U_0 and the concentration distribution in the bank regions (Figure 1). Note that neglecting these effects is equivalent to set $U_0 = D_0 = 1$, such that $K_0 = 0$. It is also easy to demonstrate that the $O(\nu)$ correction K_1 is identically zero. Indeed, $\mathcal{A}_1 = 0$, and the various integrals involve products of even ($1 - U_0$, D_0, g_{10}) and odd (D_1, U_1, g_{11}, n) functions that, integrated across a symmetrical section, yields a zero contribution. Finally, the $O(\nu^2)$ term K_2 includes the effects of the near bank velocity and concentration gradients, mainly represented by the first integral on the right hand side of equation (33), and those due to the complex structure of the flow field, the bed topography and the spatial distribution of the concentration induced by the meandering stream. The former contribution to K_2 is likely of minor importance when dealing with wide and shallow sections (i.e., with large

β), as often occurs in alluvial rivers and, in the following will be neglected in order to keep the model at the lower level of complexity. In fact, as it will be seen in the next section, the solution of the flow field in a meandering channel is available in closed form only by neglecting the boundary layers that form near to the banks (*Frascati and Lanzoni*, 2013).

The functions $g_{1i}(s,n)$ $(i=0,1)$ that describe the cross sectional distribution of c are obtained by solving the partial differential equations that arise by substituting from (28) and (29) into (25). They read:

$$\gamma D_0 U_0 \frac{\partial g_{1i}}{\partial s} - \frac{\partial}{\partial n}\left(D_0 k_{n0} \frac{\partial g_{1i}}{\partial n}\right) = f_{1i}(s,n) \qquad i=0,1 \tag{34}$$

and are subject the constraints that $\partial g_{1i}/\partial n = 0$ at the walls and

$$\int_{-1}^{1} D_0 < g_{1i} > dn = b_{1i} \quad with \quad b_{10}=0, \quad b_{11} = -\int_{-1}^{1} < g_{10}(D_1 + D_0 n\mathcal{C}) > dn. \tag{35}$$

The forcing terms f_{1i} are obtained recalling the expression of the metric coefficient h_s, and read:

$$\begin{aligned} f_{10} &= D_0(1-U_0) & (36)\\ f_{11} &= (n\mathcal{C} - U_1 - U_0\mathcal{A}_1) + D_1(1-U_0) - \gamma\, D_0 V_1 \frac{dg_{10}}{\partial n} + \\ &- \frac{\partial}{\partial n}[(k_{n1} + n\mathcal{C}k_{n0})D_0 + k_{n0}D_1)\frac{dg_{10}}{dn}] & (37)\end{aligned}$$

where $k_{ni} = D_i$, having assumed that $k_n^* = (e_t + k_t)u_{fu}^* D^*$ (*Deng et al.*, 2001).

The solution of the boundary value problems given by (34) and its constraints is in general given by the sum of a homogeneous solution, common to any order of approximation, and a particular solution related to the forcing term f_{1i}. The homogeneous solution can be written in term of Fourier series, and generally depends on the transverse distribution of concentration at the injection section. However, in the case of a sudden release of contaminant treated here, it tends to decrease exponentially with the coordinate s and, hence, vanishes far downstream of the input section (*Smith*, 1983). This condition is equivalent to impose that the $O(\epsilon)$ and $O(\epsilon^2)$ pollutant fluxes vanish ($\int_{-1}^{1} DUg_i dn = 0$ for i =1,2), as required in the derivation of equation (23).

Finally, note that, for the uniform flow in a straight channel, the along channel gradient of g_{10} is identically zero and (34) yields the classical relation (*Fischer*, 1967, 1973; *Rutherford*, 1994):

$$g_{10}(n) = \int_{-1}^{n} \left[\frac{1}{D_0\, k_{n0}} \int_{-1}^{n_1} D_0(U_0 - 1)\, dn_2 \right] dn_1 + \alpha_0 \tag{38}$$

where the constant α_0 allows g_{10} to satisfy the integral condition (35), but does not give any contribution to K_0.

3. Depth averaged flow field in alluvial channels

The characteristics of the steady flow that establishes in alluvial channels are determined by the form of the cross section and the planform configuration of the channel. The governing two-dimensional equations of mass and momentum conservation are in general obtained by depth-averaging the corresponding three-dimensional equations, and by accounting for the dynamic effects of secondary flows induced by curvature and of the boundary layers that form near to the channel banks.

The complexity of the problem prevents the derivation of general solutions in closed form. Also numerical solutions are non straightforward, owing to the difficulty of modeling secondary circulations (*Bolla Pittaluga and Seminara*, 2011). However, the governing equations can be linearized in the presence of gently sloping channel banks and meandering channels with wide and long bends, such that the flow field can be solved by perturbing the uniform flow solution in terms of two small parameters δ and ν. We resort just to these solutions, which have the pratical advantage to explicitily account, although in a simplified form, for the effects excerted on the basic flow field by the bank shape and the channel axis curvature. We then estimate analytically the longitudinal dispersion coefficient through (31) and (33).

In the following, we first derive the cross-sectional distribution of the longitudinal velocity U_0 in a straight channel with gently sloping banks (small δ). Next, we briefly recall the structure of U_1 in wide and long meander bends (small ν) with either an arbitrary or a regular distribution of the channel axis curvature.

3.1. Straight channels

The uniform turbulent flow field that establishes throughout a cross section of a straight channel can be conveniently studied introducing the local orthogonal coordinate system (s^*, σ^*, ζ^*), where s^* is the longitudinal (in this case straight) coordinate (directed downstream), σ^* is the transverse curvilinear coordinate aligned along the cross-section profile (with origin at the channel axis), and ζ^* is the coordinate normal to the bed (pointing upward) (see Figure 1c). The curvilinear nature of σ^* is accounted for through the metric coefficient:

$$h_\sigma = 1 + \frac{\zeta^*}{\cos\varphi}\frac{\partial^2 D_0^*}{\partial \sigma^{*2}}, \qquad \cos\varphi = \sqrt{1 - \left(\frac{\partial D_0^*}{\partial \sigma^*}\right)^2}, \tag{39}$$

with $D_0^*(\sigma^*)$ the local value of the flow depth, φ the angle that the vertical forms with ζ^*, and $D_z^* = D_0^*/\cos\varphi$ the flow depth measured normally to the bed (Figure 1).

The uniform character of the flow implies, on average, the flow characteristics do not vary in time and along the direction s^*. Hence, denoting by $u^*(\sigma^*, \zeta^*)$ the corresponding component of the velocity, the longitudinal momentum equation, averaged over the turbulence, reads (Appendix A):

$$S\, h_\sigma\, g + \frac{\partial}{\partial \sigma^*}\left(\frac{\nu_T^*}{h_\sigma}\frac{\partial u^*}{\partial \sigma^*}\right) + \frac{\partial}{\partial \zeta^*}\left(\nu_T^* h_\sigma \frac{\partial u^*}{\partial \zeta^*}\right) = 0, \tag{40}$$

where ν_T^* is the eddy-viscosity used to express the turbulent Reynolds stresses through the Boussinesq approximation.

In general, the channel cross section is assumed to consists of (Figure 1c): i) a central region of width $2B_c^*$ and constant depth depth D_c^*, and ii) two bank regions, each one characterized by a width (B^*-B_c^*) and wetted perimeter P_0^*. In natural channels the flow depth is usually much smaller than the wetted perimeter and, consequently the dimensionless parameter

$$\delta = \frac{D_u^*}{P_0^* + B_c^*} \tag{41}$$

is small. We will take advantage of this for solving equation (40). To this aim, we introduce the scaling:

$$\zeta = \frac{\zeta^*}{D_z^*(\sigma^*)}, \quad \sigma = \frac{\sigma^*}{P_0^* + B_c^*}, \quad D_0 = \frac{D_0^*}{D_u^*}, \quad u = \frac{u^*}{u_{fu}^*}, \tag{42}$$

$$\nu_T = \frac{\nu_T^*}{D_u^* u_{fu}^*}, \quad u_f = \frac{u_f^*}{u_{fu}^*}, \tag{43}$$

where $u_f^* = (gD_0^*S)^{1/2}$ is the local value of the friction velocity, related to the local bed shear stress τ_b^* by the relation $u_f^* = (\tau_b^*/\rho)^{1/2}$. Note that, having normalized ζ^* with D_z^*, it turns out that:

$$\frac{\partial}{\partial \zeta^*} = \frac{1}{D_z^*}\frac{\partial}{\partial \zeta}, \qquad \frac{\partial}{\partial \sigma^*} = \frac{1}{P_0^* + B_c^*}\left(\frac{\partial}{\partial \sigma} - \zeta F_1 \frac{\partial}{\partial \zeta}\right), \tag{44}$$

with

$$F_1 = \frac{1}{D_0}\frac{\partial D_0}{\partial \sigma}\left[1 + \frac{\delta^2 D_0\,(\partial^2 D_0/\partial \sigma^2)}{1 - \delta^2\,(\partial D_0/\partial \sigma)^2}\right]. \tag{45}$$

Substituting (42) and (43) into (40), the dimensionless longitudinal momentum equation results:

$$\frac{1}{D_z^2}\frac{\partial}{\partial \zeta}\left[h_\sigma \nu_T \frac{\partial u}{\partial \zeta}\right] + \delta^2\left(\frac{\partial}{\partial \sigma} - \zeta F_1 \frac{\partial}{\partial \zeta}\right)\left[\frac{\nu_T}{h_\sigma}\left(\frac{\partial}{\partial \sigma} - \zeta F_1 \frac{\partial}{\partial \zeta}\right) u\right] + h_\sigma = 0 \tag{46}$$

Under the assumption that the transverse slope of the channel bank varies slowly, such that the normals to the bed do not intersect each other, it is possible to express the dimensionless eddy viscosity ν_T as:

$$\nu_T(\zeta) = u_f\, D_z\, \mathcal{N}(\zeta), \tag{47}$$

The simplest model for the function $\mathcal{N}(\zeta)$ is that introduced by *Engelund* (1974), whereby $\mathcal{N} = 1/13$. In the following, we will adopt this scheme which allows for an analytical solution of the problem, and, as shown by *Tubino and Colombini* (1992), leads to results that agree both qualitatively and quantitatively with those obtained with a more accurate model for the function $\mathcal{N}(\zeta)$. Under the assumption of a constant $\mathcal{N}$, a slip condition has to be imposed at the bed, such that:

$$u|_{\zeta=0} = u_f \left[2 + 2.5\, ln\, \left(\frac{D_z}{d_{gr}}\right)\right]. \tag{48}$$

The other two boundary conditions to be associated to equation (46) require that the dimensionless shear stress vanishes at the water surface and equals u_f at the bed:

$$\left[\nu_T \left(\frac{1}{D_0}\frac{\partial u}{\partial \zeta} - \frac{\delta^2}{h_\sigma}\frac{\partial u}{\partial \sigma}\right)\right]_{\zeta=1} = 0, \qquad \left[\frac{\nu_T}{D_z}\frac{\partial u}{\partial z}\right]_{\zeta=0} = u_f^2. \tag{49}$$

The presence of the small parameter δ allows the expansion of the flow variables as:

$$\left(u, u_f\right) = \left(u_0, u_{f0}\right) + \delta^2 \left(u_1, u_{f_1}\right) + \mathcal{O}(\delta^4). \tag{50}$$

The cross sectional distribution $u(\sigma, \zeta)$ of the longitudinal velocity is obtained by substituting this expansion into equations (46), (48) and (49), by collecting the terms with the same power of δ^2, and by solving the resulting differential problems (see Appendix A). Integrating u along the normal ζ to the bed, the local value $U_0(\sigma)$ of the depth-averaged longitudinal velocity results:

$$U_0 = U_{00} + \delta^2\, U_{01} + O(\delta^4) \tag{51}$$

where U_{00} is a function of the local flow depth $D_0(\sigma)$ and the relative grain roughness d_{gr}, while U_{01} depends also on $\partial D_0/\partial\sigma$ (i.e., the local slope) and $\partial^2 D_0/\partial\sigma^2$ (Appendix A).

The cross sectional distribution of U_0 needed to compute the longitudinal dispersion coefficient is then determined by specifying the relative bed roughness

d_{gr} and, more importantly, the across section distribution of the flow depth $D_0(\sigma)$. In the absence of experimental data, we need to describe the bank geometry. Here, we propose to handle empirically the problem assuming a transverse distribution of the flow depth of the form:

$$D_0^*(\sigma) = D_c^*\, erf\Big[\beta_f (\, 1 - \sqrt{|\sigma|}\,)\Big], \qquad \sigma \in [-1, 1], \tag{52}$$

with β_f a shape parameter measuring the steepness of the banks. Note that, according to (52), $erf(\beta_f)$ should be equal to 1 in order to ensure that $D_0^*(0) = D_c^*$. The latter requirement is fulfilled only asymptotically, for β_f tending to infinity. For this reason, in the following we will consider only values of $\beta_f \geq erf^{-1}(0.999) = 2.32675$, corresponding to $D_c^* < D_0^*(0) \leq 0.999 D_c^*$. Note also that β_f is related to the parameter $\delta\beta_c$ through the relation:

$$\delta\, \beta_c = \left[1 - \frac{erf^{-1}(0.999)}{\beta_f}\right]^2 \tag{53}$$

where $\beta_c = B_c^*/D_u^*$ and having assumed $D_0^*(B_c^*) \simeq 0.999 D_c^*$. As β_f increases also $\delta\beta_c$ increases, resulting in progressively steeper cross sections (Figure 2a)). Note that increasing values of δ imply higher bank slopes. In the limit of $\beta_f = 2.32675$, it results $\delta\beta_c$ equal to 0, corresponding to $B_c^* = 0$ (no central region), while as $\beta_f \to \infty$, the classical rectangular cross-sectional configuration (P_0^*=0) is recovered (Figure 2a).

Interestingly, the distributions of $u_{f1}(\sigma)$ shown in Figure 2b indicate an increase of the friction velocity u_f, with respect to the uniform flow, in the steeper portion of the bank, and a corresponding decrease in the part of the bank adjacent to the central region. This trend, due to the longitudinal momentum transfer from the center of the cross section (where flow velocities are higher) to the banks, implies that the channel can transport sediments even though the bank toes are stable. Note also that $u_{f1}(\sigma)$ vanishes towards the center of the cross section, where the bottom is flat, and at the outer bank boundary, where D_0 tends to zero.

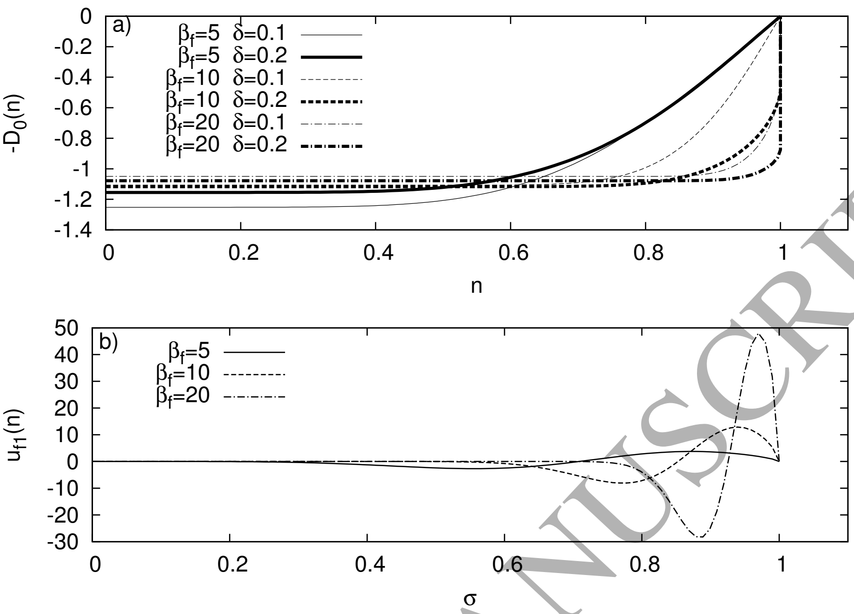

Figure 2: (a) Cross-sectional bed profile for various β_f and for $\delta = 0.1$ and $\delta = 0.2$. (b) Cross-section distributions along σ coordinate of the $\mathcal{O}(\delta^2)$ corrections provided to the dimensionless friction velocity u_{f1}, for the values of β_f considered in plot a) and for $d_{gr} = 0.02$.

3.2. Meandering channels

The flow field that takes place in a meandering channel with a compact cross section is strictly related to the secondary flow circulations driven by the curvature of streamlines and the deformation of the channel bed, which generally exhibits larger scours in the correspondence of the outer bank of a bend (*Seminara*, 2006). Although numerical models have the advantage to overcome the restrictions affecting theoretical analyses (e.g., linearity or weak non-linearity, simplified geometry) they still require a large computational effort to correctly include the effects of secondary helical flow and to reproduce the bed topography of movable bed channels (*Bolla Pittaluga and Seminara*, 2011; *Eke et al.*, 2014). That is why linearized models have been widely adopted to investigate the physics of river meandering (*Seminara*, 2006), the long-term evolution of alluvial rivers (*Howard*, 1992; *Frascati and Lanzoni*, 2009; *Bogoni* *et al.*, 2017), and the possible existence of a scale invariant behavior (*Frascati and Lanzoni*, 2010). These models, owing to their analytical character, not only provide insight on the basic mechanisms operating in the process under investigation, but also allow to develop relatively simple engineering tools which can be profitably used for practical purposes.

In the following we refer to the linearized hydro-morphodynamic model developed by *Frascati and Lanzoni* (2013) that, in the most general case, can manage also mild along channel variations of the cross section width. The model is based on the two-dimensional, depth-averaged shallow water equations, written in the curvilinear coordinates s, n and, owing to the large aspect ratio β usually observed in natural rivers, neglects the presence of the near bank boundary layers. The flow equations, ensuring the conservation of mass and momentum and embedding a suitable parametrization of the secondary flow circulations, are coupled with the two-dimensional sediment balance equation, complemented with the relation describing the rate of sediment transport. The solution of the resulting set of partial differential equations takes advantage of the fact that, in natural channels, the curvature ratio ν is small (ranging in the interval 0.1-0.2), and assume that flow and topography perturbations originating from deviations of the channel planform from the straight one are small enough to allow for linearization. In the case of a constant width rectangular section (for which $D_c^* = D_u^*$), the dimensionless flow field yields:

$$(U, D) = (1, 1) + \nu(U_1, D_1) + O(\nu^2) \tag{54}$$

where

$$\begin{aligned} U_1(s,n) &= \sum_{m=0}^{\infty} u_{c_m} \sin(M_c n) \\ D_1(s,n) &= (\overline{h}_1 \mathcal{C} + \overline{h}_2 \mathcal{C}' + \overline{h}_3 \mathcal{C}'')\, n + \sum_{m=0}^{\infty} d_{c_m} \sin(M\, n) \end{aligned} \tag{55}$$

Here, $\mathcal{C}(s)$ is the local curvature of the channel, $\mathcal{C}'(s)$ and $\mathcal{C}''(s)$ its first and second derivatives, $\overline{h}_i$ and $\overline{d}_i$ $(i = 1, 3)$ are constant coefficients, $M =$

$(2m+1)\pi/2$, and $u_{c_m}(s)$, $d_{c_m}(s)$ are functions of the longitudinal coordinate s:

$$
\begin{aligned}
u_{c_m} &= \sum_{j=1}^{4} c_{c_{mj}}\, e^{\lambda_{c_{mj}} s} + A_{c_m} \sum_{j=1}^{4} \left[g_{c_{j0}} \int_0^s \mathcal{C}(\xi)\, e^{\lambda_{c_{mj}}(s-\xi)} d\xi + g_{c_{j1}} \mathcal{C} \right] \\
d_{cm} &= \sum_{j=1}^{4} d_{mj} \frac{d^{j-1} u_m}{ds^{j-1}} + A_m \sum_{j=1}^{5} d^c_{mj} \frac{d^{j-1}\mathcal{C}}{ds^{j-1}}
\end{aligned}
\qquad (56)
$$

We refer the interested reader to *Frascati and Lanzoni* (2013) for further details about the model, its derivation and implementation, while all the coefficients needed to compute U_1 and D_1 are reported in the Supplementary Information. It is worthwhile to note that the relevant dimensionless parameters (geometric, hydraulic and sedimentological) needed as input data to the model are the width to depth ratio β, the dimensionless grain size d_{gr}, and the Shields parameter for the uniform flow conditions, τ_{*u}.

The expressions (54) are used to compute the forcing term f_{11}, needed to solve the boundary value problem (34) for g_{11}. Note that by substituting (54) into (38) yields $g_{10} = 0$ (owing to the neglecting of bank effects). The particular solution of (34) is obtained by writing the forcing term as $f_{11} = p(s)q(n)$ (i.e., separating the variables through Fourier series), and by introducing the appropriate Green function (*Morse and Feshbach*, 1953). We obtain:

$$
g_{11}(s,n) = \frac{1}{\gamma} \sum_{m=0}^{\infty} (-1)^{m+1} \cos[\mu_{2m+1}(n+1)] \int_0^{s-s_0} p_m(s-\chi)\, e^{-\mu_{2m+1}^2 \chi/\gamma} d\chi \qquad (57)
$$

where $\mu_m = m\pi/2$,

$$
p_m(s) = \frac{2}{M_c^2}(-1)^m \mathcal{C}(s) - u_{c_m}(s), \qquad (58)
$$

and s_0 denotes the position of the injection section. By assumption, the length scale over which the contaminant cloud has evolved, L_c^*, is well in excess of the transverse mixing distance, $\sim U_0^* B^{*2}/k_n^*$. Consequently, the position s_0 of the injection section can be set arbitrarily far upstream, taking $s_0 = -\infty$.

Physically, this is equivalent to assume that the solution depends only on values of $p(s-\chi)$ upstream of s over a diffusion length scale. Indeed, the integral with respect to the dummy variable χ decays as $\exp(-\mu_m^2 \chi/\gamma)$, and hence depends on the values of p closest to s.

The solution (57) is in general valid for an arbitrary, although slowly varying, spatial distribution of the channel axis curvature. It takes a particularly simple form in the schematic case of a regular sequence of meanders with the axis curvature described by the sine generated curve $\mathcal{C}(s) = e^{2\pi\imath s} + c.c.$ (*Leopold et al.*, 1964), where i is the imaginary unit, and c.c. denotes complex conjugate. In this case the flow field reads (*Blondeaux and Seminara*, 1985):

$$\begin{aligned} U_1(n) &= [d_{u0}n + d_{u1}sinh(\Lambda_1 n) + d_{u2}sinh(\Lambda_2 n)]e^{2\pi i s} + c.c. \\ D_1(n) &= [d_{d0}n + d_{d1}sinh(\Lambda_1 n) + d_{d2}sinh(\Lambda_2 n)]e^{2\pi i s} + c.c. \end{aligned} \tag{59}$$

The constant coefficients $d_{uj}, d_{dj} (j = 0, 1, 2)$, Λ_1, Λ_2 (reported in the Supplementary Information) depend on β, d_{gr}, τ_{*u}, and λ. The above relationships indicate that both the flow depth and the velocity tend to increase towards the outside channel bank. The deepening of the outer flow that takes place in a movable bed, in fact, pushes the thread of high velocity towards the outside bank, unlike in the fixed bed case, where the predicted thread of high velocities is located along the inside of the bend.

The forcing term $f_{11} = n\mathcal{C} - U_1$ can thus be written as $f_{11} = p(s)q(n) + c.c.$, with $p(s) = e^{2\pi i s}$ and $q(n) = n - d_{u0}n - d_{u1}sinh(\Lambda_1 n) - d_{u2}sinh(\Lambda_2 n)$. It follows that:

$$g_{11}(s,n) = \frac{1}{\gamma}\sum_{m=0}^{\infty}\frac{b_m}{2\pi\imath + M^2/\gamma}\cos[M\,(n+1)]\;e^{2\pi\imath s} + \;c.c. \tag{60}$$

where b_m are constant coefficients (see Supplementary Information). Substituting (60) into (33) and recalling (24) we finally obtain the relationship giving the bend averaged $O(\nu^2)$ correction to the longitudinal dispersion coefficient associated with a regular sequence of meanders:

$$K = \nu^2 \sum_{m=0}^{\infty} M^2 \frac{b_m \tilde{b}_m}{M^4 + (2\pi\gamma)^2} \tag{61}$$

where a tilde denotes complex conjugate.

4. Comparison with tracer field data

4.1. The considered dataset

In order to test the validity of the proposed theory, we need information not only on the dispersion coefficient and the average hydrodynamic properties of the considered river reach, but also on the planform shape of the channel, on the geometry of the cross sections and, possibly, on the cross sectional velocity distribution. Despite the numerous tracer experiments carried out on river dispersion (*Seo and Cheong*, 1998; *Nordin and Sabol*, 1974; *Yotsukura et al.*, 1970; *McQuivey and Keefer*, 1974), only a few report also this type of information. In particular, the data collected by *Godfrey and Frederick* (1970) include the time distribution of the local tracer concentration C at a number of monitoring section and the cross-section distributions of the flow depth, $D^*(n^*)$, and of the vertical profiles of the longitudinal velocity $u^*(n^*, z^*)$. This dataset therefore provides all the information needed to assess the robustness of the present modeling framework. In each test a radiotracer (gold-198) was injected in a line source across the stream. About 15 ml of the tracer, a highly concentrated solution of gold chloride in nitric and hydrochloric acid, was diluted to a volume of 2 l. The injection was made at a uniform rate over a 1-minute period. The concentration of radionuclide used in each test was proportional to the discharge (about 2,6 GBq $m^{-3}s^{-1}$). The concentrations near to the stream centerline were observed by a scintillation detector. The resolving time for the entire system was found to be 50 s. The error due to the resolving time is about 5-10%.

Among the five river reaches considered by *Godfrey and Frederick* (1970), three exhibit almost straight planforms: the Copper Creek below gage (near

Gate City, Va), the Clinch River above gage (hereafter Clinch River a.g., near Clinchport, Va), and the Clinch River below gage (hereafter Clinch River b.g., near Speers Ferry, Va). The other two river reaches, the Powell River near Sedville (Tenn) and the Copper Creek above gage (near Gate City, Va) have meandering planforms. These latter data have been integrated with the estimates of K^* obtained from tracer tests carried out in other five straight and eight meandering rivers, namely the Queich, Sulzbach and Kaltenbach rivers (*Noss and Lorke.*, 2016), the Ohio, Muskegon, St. Clair and Red Cedar rivers (*Shen al.*, 2010), the Green-Duwamish River (*Fischer*, 1968), the Missouri River (*Yotsukura et al.*, 1970), the Lesser Slave River (*Beltaos and Day*, 1978), and the Miljacka River (*Dobran*, 1982). Figure 3 shows the planform configurations of the investigated reaches, extracted from topographic maps, while the geometrical, hydraulic and sedimentologic parameters of each stream are reported in Table 2. In particular, the curvature ratio ν and the wavenumber λ have been determined from the spatial distribution of channel axis curvature through the automatic extraction procedure described by *Marani et al.* (2002). The mean grain size estimates have been obtained on the basis of information available from literature (*Godfrey and Frederick*, 1970; *Yotsukura et al.*, 1970; *Beltaos and Day*, 1978), from the USGS National Water Information System [http://waterdata.usgs.gov/nwis], or from direct inspection (Dobran 2007, personal communication). In addition to real meandering stream data, Table 2 reports the laboratory data characterizing the longitudinal dispersion experiment carried out by *Boxall and Guymer* (2007) in a flume with a sine generated meandering planform and a sand bed that was artificially fixed by chemical hardening after the initially uniform trapezoidal cross section was shaped by the flow.

For a given test i, we used the data collected by *Godfrey and Frederick* (1970) to compute at each monitored cross section j the area A^*_{ij} and the total wetted perimeter P^*_{ij}. We then used the cross sectional velocity data $u^*_{ij}(n^*, z^*)$ to compute the depth averaged velocity $U^*_{ij}(n^*)$ and the flow discharge Q^*_{ij}. All the relevant quantities deduced from the experimental dataset are collected in

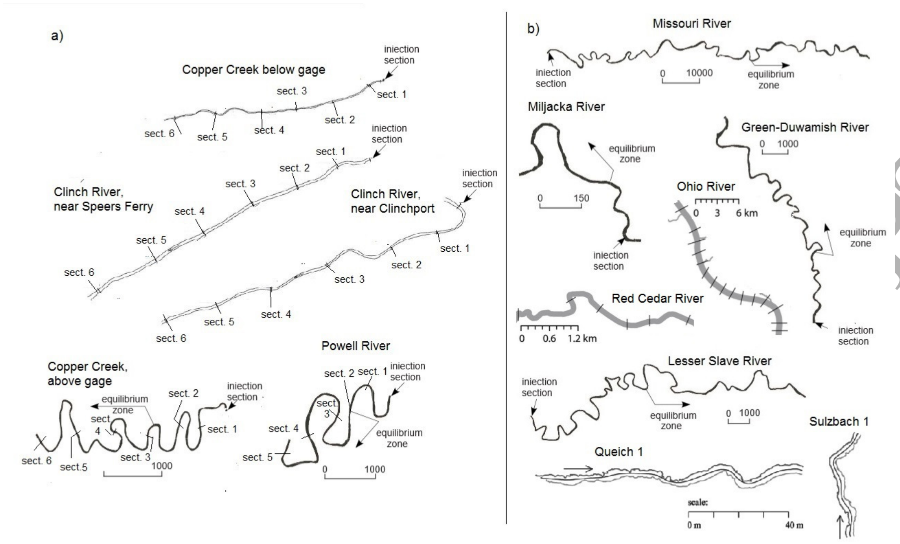

Figure 3: a) Plan view of the river reaches investigated by *Godfrey and Frederick* (1970) and location of the monitored cross sections. b) Planforms of further meandering streams (*Fischer*, 1968; *Yotsukura et al.*, 1970; *Beltaos and Day*, 1978; *Dobran*, 1982; *Shen al.*, 2010; *Noss and Lorke.*, 2016) considered for testing the present theoretical approach.

Table S1 reported in the Supplementary Information. In particular, the values of the mean slope are those provided directly by *Godfrey and Frederick* (1970), while the friction velocities have been estimated under the hypothesis of a locally uniform flow field.

The dispersion coefficients estimated by *Godfrey and Frederick* (1970) have been obtained by applying the method of moments. However, the presence of a relatively long tail in the temporal distribution of the concentration (Figure 4a) and the sensitivity of small concentrations to measurement errors limit the accuracy of this method (*Rutherford*, 1994). For this reason, we have recalculated the dispersion coefficients by considering the Chatwin's method (*Chatwin*, 1980), which has also the advantage to give an indication whether a monitoring section is located or not whitin the equilibrium region, where a Fickian dispersion model can be applied. Figure 4b shows an example of the application of the method to the tracer data collected in the Clinch Creeek (test T10). The

Chatwin method introduces the transformed variable $\hat{C}(t^*)$, defined as:

$$\hat{C} = \pm\sqrt{t^* \ln \frac{C_{max}\sqrt{t^*_{max}}}{C\sqrt{t^*}}} \tag{62}$$

where $C = C(s^*_j, t^*)$ is the temporal distribution of the cross-sectionally averaged concentration measured a the j-th cross section, C_{max} is the corresponding peak concentration, t^*_{max} is the peaking time, and the $+$ and $-$ signs apply for $t^* \leq t^*_{max}$ and $t^* > t^*_{max}$, respectively. In the transformed plane $\hat{C}, t^*$, a temporal distribution of tracer concentration following a Gaussian behavior should plot as a straight line. The slope $-0.5\,(Q^*/A^*_j)\,/\sqrt{K^*_j}$ and the intercept $0.5\,x^*_j\,/\sqrt{K^*_j}$ of this line allow one to estimate the dispersion coefficient $\sqrt{K^*_j}$ and the cross sectionally averaged velocity Q^*/A^*_j.

The data suggest that, for all the sections, only the rising limb and the near peak region of the concentration time distribution are approximately linear, and hence can be described by a Gaussian distribution. Conversely, a departure from the linear trend is evident in the correspondence of the tails, indicating a deviation from the Fickian behavior.

The values of K^*_j estimated by considering the linear part of $\hat{C}(t^*)$ for all the data collected by *Godfrey and Frederick* (1970) turn out invariably smaller than those calculated according to the method of moments (see Table S2 of the Supplementary Information). In order to assess the sensitivity of these estimates to the method used to derive them, we applied also the routing method based on the Hayami solution (*Rutherford*, 1994). This method, provided that the dynamics of the cross-sectionally averaged concentration is Gaussian, takes advantage of the superimposition of effects to determine the temporal distribution of C in a section, given the local values of U^*, K^* and the concentration-time curve in an upstream section.

The resulting solution has the advantage that it can be used to route downstream a given temporal distribution of concentration without invoking the frozen cloud approximation. In fact, for moderately large values of s^* and t^* it gives a concentration profile similar to that provided by the classical Taylor

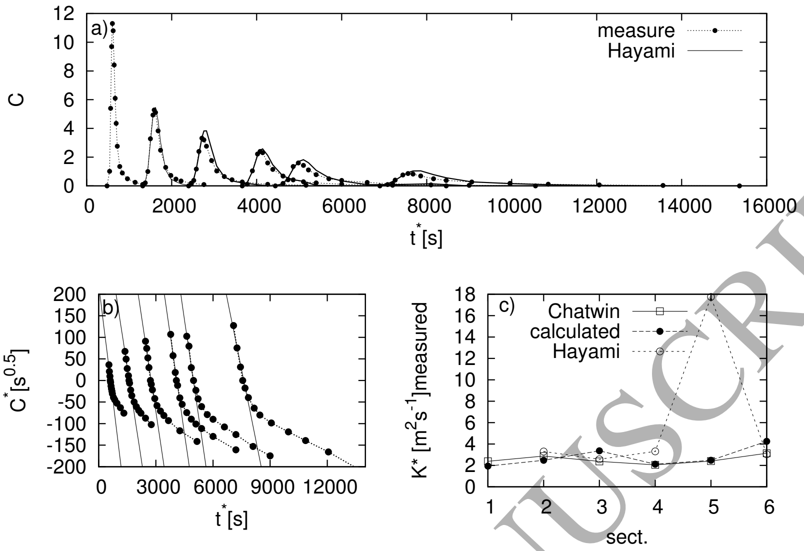

Figure 4: a) Temporal distributions of the concentration measured by *Godfrey and Frederick* (1970) in the tracer test T10 carried out along the Clinch River b.g.: black circles indicate the measured concentration; continuous lines denote the concentration profiles predicted by applying the Hayami's calibration method. b) The Chatwin's transformation is applied to the data shown in a): black circles indicate the measured data; continuous straight lines are regression lines fitted to concentrations near the peak. c) Comparison between the dispersion coefficients estimated by means of the present theoretical approach and Chatwin and Hayami methods.

solution. For all the monitored sections, except the first one, it is thus possible to estimate the values of U^* and K^* which ensure the best agreement between the measured and predicted concentration profiles. Figure 5 shows the results of the application of the Chatwin and Hayami methods. In some cases the Hayami method tends to yield larger values of K^*. Possible reasons of this behaviour are the pour fitting of the routed solutions and the significance of the tail owing to the entrapment and retarded release of the tracer into dead zones, absorption on sediment surfaces, hyporheic fluxes.

Nevertheless, the most significant differences between the two approaches generally occurs in sections where the estimate deviates significantly (longer error bars in Figure 5a) from the average value in the considered river reach, i.e. where the dynamic of the tracer cloud is likely influenced by some localised effect, such as irregularities along the channel sides, or the channel bed, determining the retention of a certain amount of tracer. On the other hand, the average velocity estimated with the two methods are very similar (Figure 5b). In the following, we will consider the estimates of the dispersion coefficients provided by the Chatwin method when referring to the measured values of K^*.

4.2. Comparison with straight river dispersion data

Before pursuing a comparison between observed and predicted dispersion coefficients, it is worthwhile to test the reliability of the flow field model described in Section 3.1. Figure 6 shows the cross sectional distribution of the flow depth (left panels) and depth averaged velocity (right panels) measured by *Godfrey and Frederick* (1970) in six locations along the Clinch River b.g. (test T10). The theoretically predicted velocities, shown in Figure 6, have been obtained either by introducing into equation (51) the observed flow depth, or by considering the simplified cross sectional geometry described by equation (52) and selecting the value of β_f which better interpolates the measured depth profile. The agreement between measured and computed velocity distributions is in general reasonably good (correlation coefficient, $R_U^2 = 0.81$).

The comparison between the estimates of K^* obtained from the tracer data of *Godfrey and Frederick* (1970) and those predicted by inserting in equation (31) the flow field described by equation (51) are shown in Figure 7a. Figures 7a) and b) also show in white squares a comparison between the dispersion coefficients evaluated according to the present theoretical approach and those estimated from measurements by *Noss and Lorke.* (2016) and *Shen al.* (2010) for the Queich, Sulzbach, Kaltenbach, Muskegon Rivers.

The theoretical estimates are reasonably good, with about 70% of predictions ensuring an error smaller than ±30% (dotted lines in Figure 7a). Overall, the model tends to underestimate the dispersion coefficient for the larger values of K^*, which, usually occour in the most distant sections from the injection, where

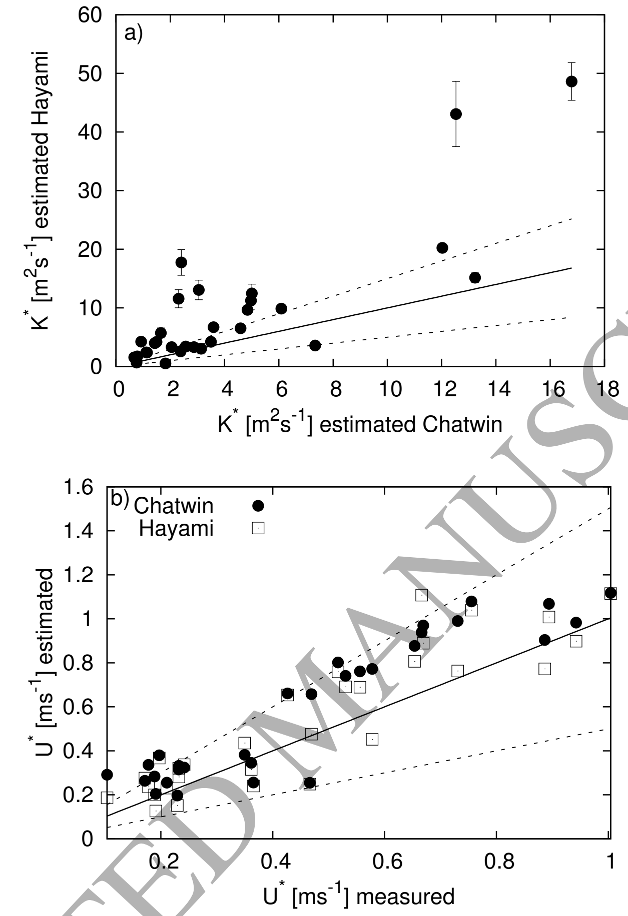

Figure 5: a) The dispersion coefficients predicted by the Hayami method are plotted versus the values provided by the Chatwin method. The error bar measures the scatter of the local value of the dispersion coefficient provided by the Haymi method with respect to the average value of each river reach. b) The average velocity values of each cross section predicted by the Hayami and Chatwin methods are plotted versus the field value. The continuous line denotes the perfect agreement; the dashed lines corresponds to a ±50 % error.

the measured concentration profiles are particularly flat.

In any case, the present estimates of K^* are definitely more accurate than those provided by other predictors available in literature, as documented by the values of the discrepancy ratios, $d_r = log(K^*_{pred}/K^*_{meas})$, plotted in Figure

7b) and 7d). To give a visual perception of the goodness of the different models, Figure 7 shows the data relative to the models displaying the best (smaller mean discrepancy ratio) and worst (larger mean discrepancy ratio) performance according to Table 1 (a Figure reporting all the data is provided in the Supplementary Information). Note that, the coefficient κ_0 of the formula proposed by *Deng et al.* (2001) and reported in Table 1, has been here reduced by 1/15. Indeed, this coefficient was originally determined by introducing a multiplicative empirical constant ψ (= 15, according to *Deng et al.* (2001)) in order to achieve a better agreement with the observed dispersion coefficients. These coefficients, at least in the specific case of the data provided by *Godfrey and Frederick* (1970), were calculated through the method of moments that, as discussed above, tend to overestimate K^* with respect to the Chatwin or the routing methods. Nevertheless, even by reducing the value of κ_0, the predictions of K^* obtained from the formula by *Deng et al.* (2001) are significantly less accurate (mean discrepancy ratio $< d_r >= 0.63$) than those resulting from the present theoretical approach ($< d_r >= 0.19$). Even worse results are attained when considering other predictors (see Table 1).

It is important to stress that the present methodology, being physically based, does not need the introduction of any fitting parameter. The input data are simply the flow discharge, the free surface channel width, the longitudinal slope, the friction velocity (strictly associated with the sediment grain size and the type of bed configuration, i.e., plane or dune covered), and the cross-sectional distribution of the flow depth or, alternatively, its simplified analytical description (equation (52)). Finally, we observe that including the higher order effects that the presence of the channel banks exert on the transverse gradient of U_0 (associated to the $O(\delta^2)$ contribution in equation (51)) always leads to improve the estimate of K^* ($< d_r >= 0.190$, instead of 0.188).

Table 2: Tracer tests considered to assess the present theoretical framework. Definitions are as follows: B^*, half cross-section width; Q^*, flow discharge; S, longitudinal channel slope; δ, relative variation rate of the cross section in the transverse direction$= D^*_u/(P^*_0 + B^*_c)$; ν, curvature ratio $= B^*/R^*_0$, with R^*_0 twice the minimum radius of curvature of the channel axis within a meandering reach; λ, dimensionless meander wavenumber, $= 2\pi B^*/L^*$, with L^* the intrinsic meander length. All the quantities are averaged along the investigated river reach.

River	B^* (m)	Q^* (m^3/s)	S (%)	u^*_{fu} (m/s)	Planform	δ	ν	λ
Clinch River a.g.[1]	17.3	6.8	0.03	0.045	straight	0.032	0	-
Clinch River b.g.[2]	30	9.1,85,51	0.04	0.05,0.085,0.076	straight	0.04,0.07,0.07	0	-
Copper Creek a.g.[3]	8.5	1.5,8.5	0.13	0.08,0.104	straight	0.06,0.09	0	-
Copper Creek b.g.[4]	8.5	0.9	0.30	0.104	meandering	0.044	0.11	0.04
Powell River[5]	17.2	4	0.03	0.052	meandering	0.047	0.15	0.036
Green-Duwamish[6]	20.0	12	0.02	0.049	meandering	0.07	0.13	0.090
Lesser Slave[7]	25.4	71	0.01	0.055	meandering	0.17	0.2	0.063
Missouri[8]	90	950	0.01	0.055	meandering	0.06	0.05	0.04
Miljacka[9]	5.7	1	0.11	0.055	meandering	0.08	0.09	0.05
Exp. Flume [10]	0.5	0.025	0.12	0.031	meandering	0.19	0.08	0.157
Queich 1 [11]	1.52	0.21	0.12	0.048	meandering	0.25	0.13	0.32
Queich 2 [11]	0.95	0.25	0.19	0.068	straight	0.42	0.	-
Sulzbach 1 [11]	1.315	0.16	0.32	0.079	meandering	0.25	0.11	0.21
Sulzbach 2 [11]	0.72	0.16	0.26	0.025	straight	0.6	0.	-
Kaltenbach [11]	1.01	0.15	0.52	0.103	straight	0.4	0.	-
Muskegon [12]	35	48.41	0.6	0.24	straight	0.06	0.	-
Ohio [12]	235	1405	0.007	0.061	meandering	0.04	0.05	0.1
St Clair [12]	276.6	5000	0.088	0.083	straight	0.06	0	-
Red Cedar [12]	6.33/12.34	2.7/19.8	0.2	0.11/0.14	meandering	0.19/0.15	0.01	0.02/0.04

[1] *Godfrey and Frederick* (1970), test T5;

[2] *Godfrey and Frederick* (1970), tests T2, T7, T10;

[3] *Godfrey and Frederick* (1970), tests T1, T6;

[4] *Godfrey and Frederick* (1970), test T3;

[5] *Godfrey and Frederick* (1970), test T4;

[6] *Fischer* (1968);

[7] *Beltaos and Day* (1978);

[8] *Yotsukura et al.* (1970);

[9] *Dobran* (1982);

[10] *Boxall and Guymer* (2007);

[11] *Noss and Lorke.* (2016);

[12] *Shen et al.* (2010);

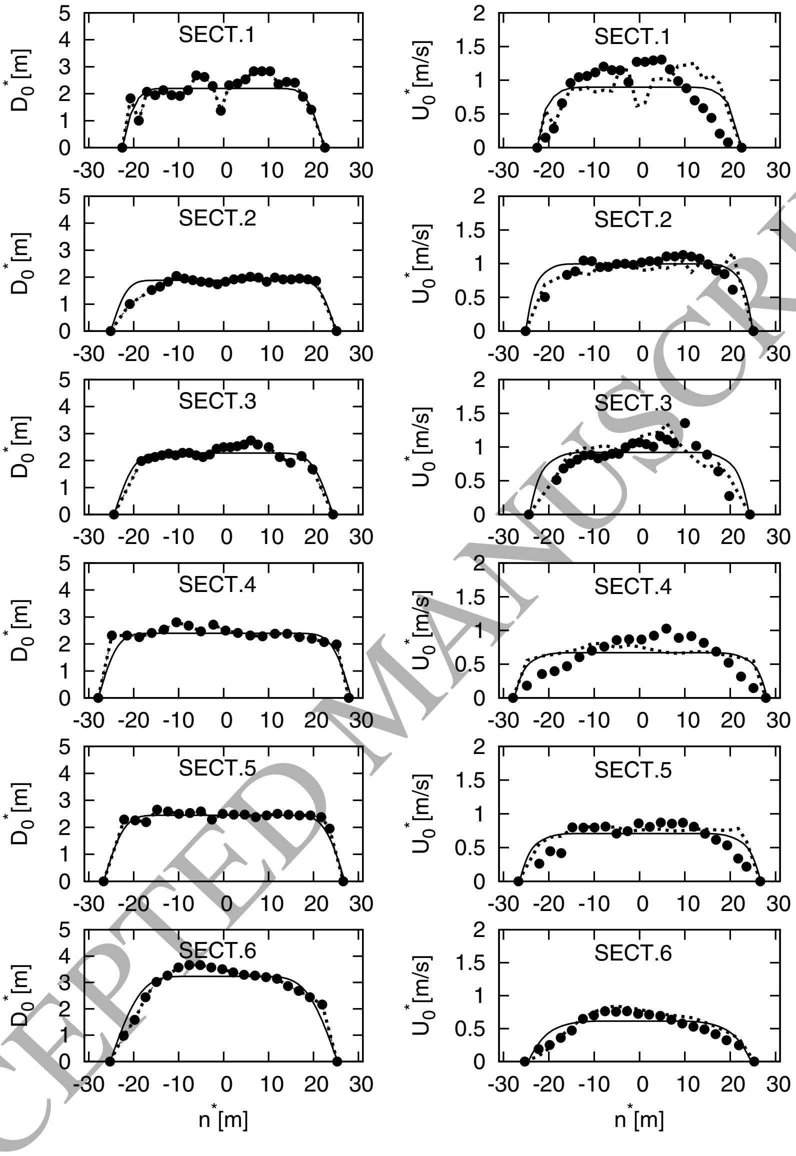

Figure 6: Cross sectional distributions of the flow depth D^* and of the depth averaged velocity U_0^* across six sections of the Clinch River b.g.. Black circles correspond to the data measured by *Godfrey and Frederick* (1970) in test T10. Continuous lines represent the smoothed cross section described by (52) and the corresponding velocity profiles ($R_D^2 = 0.95$; $R_U^2 = 0.84$). Dotted lines represent the velocity profile predicted by substituting into equation (51) the actual flow depth distributions ($R_U^2 = 0.81$).

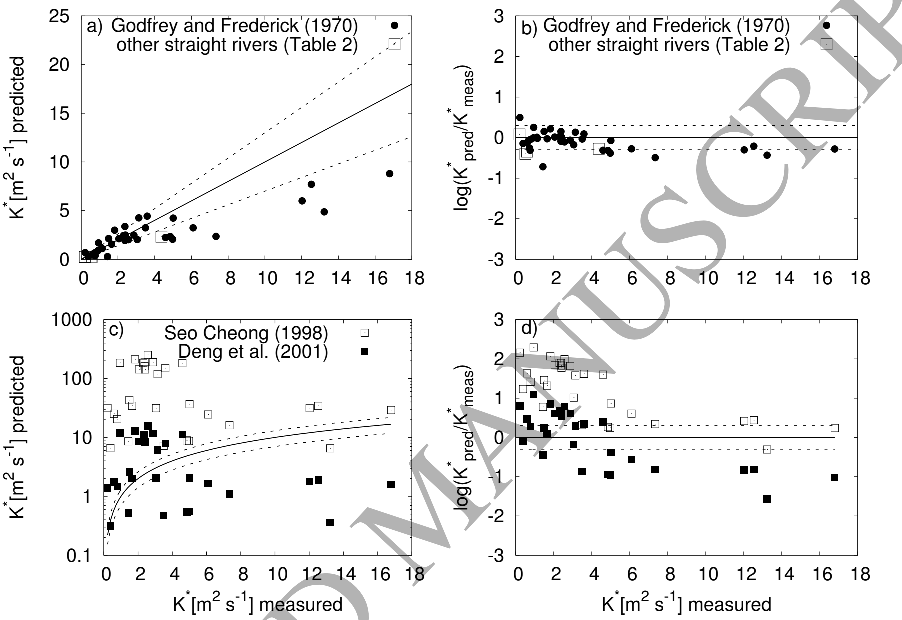

Figure 7: On the left: Comparison between the dispersion coefficients predicted theoretically and those estimated from tracer test data (*Godfrey and Frederick*, 1970) in almost straight channels by applying the Chatwin method. a) Present theoretical approach. c) *Deng et al.* (2001)'s (ψ=1) and *Seo and Cheong* (1998)'s predictors. White squares in a) are the dispersion coefficients evaluated according to the present theoretical approach versus the values estimated from measurements by *Noss and Lorke.* (2016) and *Shen al.* (2010) for the Queich, Sulzbach, Kaltenbach, Muskegon Rivers. The continuous line denotes the perfect agreement; the dotted lines corresponds to a ±30 % error. On the right: b) and d) values of the discrepancy ratio associated with the data respectively plotted in figures a) and c). The continuous line denotes the perfect agreement; the dashed lines corresponds to a ±50 % error.

4.3. Comparison with meandering river dispersion data

In the case of meandering streams, besides Q^*, B^*, S, u^*_{fu}, additional input information to the present model is the spatial distribution of channel axis curvature. These data are used to determine the dimensionless parameters β, τ_{*u}, d_{gr}, ν, as well as the along channel distribution of the channel axis curvature $\mathcal{C}\ (s)$ needed to compute the flow field through equations (55). The expressions of $U_1(s,n)$ and $D_1(s,n)$ are then employed to compute f_{11} and to solve the problem (34) for g_{11}, and, ultimately, to obtain the $O(\nu^2)$ correction (33) to the longitudinal dispersion coefficient.

In order to test the reliability of the flow field model described in Section 3.2, a comparison with the flow depths (left panels) and depth averaged velocities (right panels) measured by *Boxall and Guymer* (2007) at the apex and the cross-over sections of an experimental meandering channel is reported in Figure 8. The theoretically predicted velocities have also been compared with the velocity profiles calculated according to *Smith* (1983) for the theoretical flow depth distributions (continuos lines on the left panels):

$$U^* = \frac{D^{*0.5} U^*_u D^*_u}{H^*_u} \tag{63}$$

where H^*_u is the cross-sectional average of $D^{*1.5}$. The cross sectional shapes predicted by the present model reproduce correctly (R^2_D=0.90) the topography variations induced by alternating bends (possible departures being related to the presence of bedforms not accounted for in the model). The overall comparison appears reasonably good also in terms of depth integrated longitudinal velocities ($R^2_U = 0.93$) and the theoretically predicted profiles yield a better performance with respect to those calculated according to the approximate method proposed by *Smith* (1983) (R^2_U=0.91).

Figure 9a) shows the comparison between the bend averaged values of the longitudinal dispersion coefficient estimated from the measures carried out by *Godfrey and Frederick* (1970) in the Copper Creek and in the Powell River and those predicted by either the leading term K_0 (equation (31)) entailing a

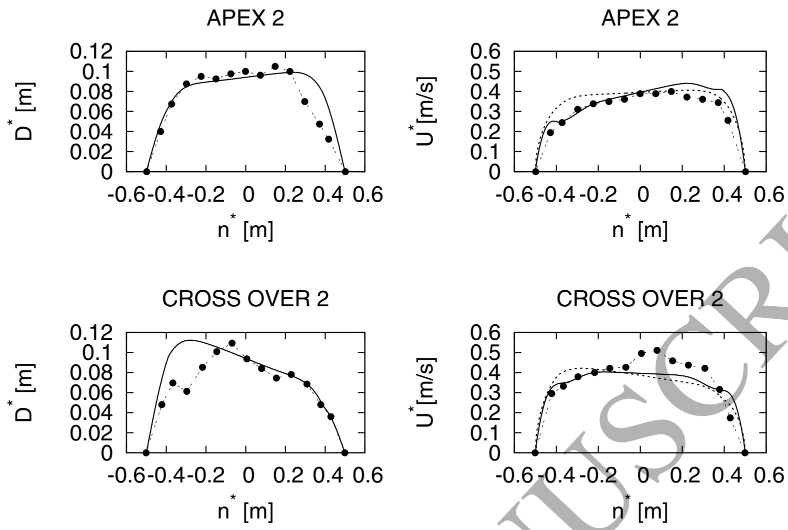

Figure 8: Cross sectional distributions of the flow depth D^* and of the depth averaged velocity U^* across two sections of the experimental meandering channel of *Boxall and Guymer* (2007). Black circles correspond to the data measured by *Boxall and Guymer* (2007). Continuous lines represent the theoretical cross section ($D_0 + \nu D_1$), described by (52) and (59), and the corresponding velocity profiles. Dotted lines represent the velocity profile predicted according to *Smith* (1983) for the theoretical flow depth distributions (continuos lines on the left panels).

straight channel, or by considering also the correction $\nu^2 K_2$ (equation (33)), accounting for the presence of river bends. This correction turns out to pick up the right order of magnitude and, on the whole, ensures a degree of accuracy greater than that attained when neglecting curvature effects ($< d_r >= 0.32$ instead of $< d_r >= 0.76$). As expected, when treating the river as straight, the predicted values of K_0^* are systematically lower than those observed in the field. In is worthwhile to note that the points corresponding to cross sections T3-S1, T3-S2 and T4-S1, for which the theory tends in any case to overestimate K^*, are quite close to the injection section and, therefore, likely fall outside the zone where a Fickian dispersion model holds.

The ability of the present theoretical framework to give robust estimates of K^* is confirmed by Figure 9b), reporting the predicted values of K^* against those resulting from the tracer test data for all the considered meandering streams. On the whole, the effect of the curvature is to slightly improve the degree of accuracy ($< d_r >= 0.22$, instead of 0.29), although sometimes the theoretical coefficients turn out to be lower than those observed in the field. This can be partly explained with the fact that the predicted $O(\nu^2)$ correction does not account for the near bank velocity gradients associated with the presence of a boundary layer and has been obtained on the basis of a linearized treatment of the flow field, which tends to underestimate the intensity of both secondary circulations and transverse bed deformations forced by the meandering stream. Clearly, a number of other processes act in the field to make dispersion not entirely Fickian, contributing to the data scatter. We return later on this issue. Finally, note that for the considered set of rivers, the results remain basically unaltered ($< d_r >=0.225$, instead of 0.22) when, instead of considering the observed spatially varying curvature signal, we consider a sequence of regular meanders with maximum curvature equal to the inverse of the mean minimum radius of curvature within the river reach.

5. Discussion

The rational perturbative framework developed in the previous sections, based on a suitable scaling of the two-dimensional advection-diffusion equation and on the introduction of a reference system, traveling downstream with the contaminant cloud, accounting for the along channel variability of the cross-sectionally averaged velocity, provides a clear picture of the processes affecting the spreading of a contaminant in alluvial rivers.

The velocity gradients that characterize the near bank regions of natural streams, where the flow depth progressively vanishes, influence the longitudinal dispersion at the leading order of approximation (equation (31)), corresponding to a straight channel planform. Secondary circulations driven by centrifugal and topographical effects typical of meandering channels provide a second order correction (equation (33)). The presence of a secondary helical flow enhances

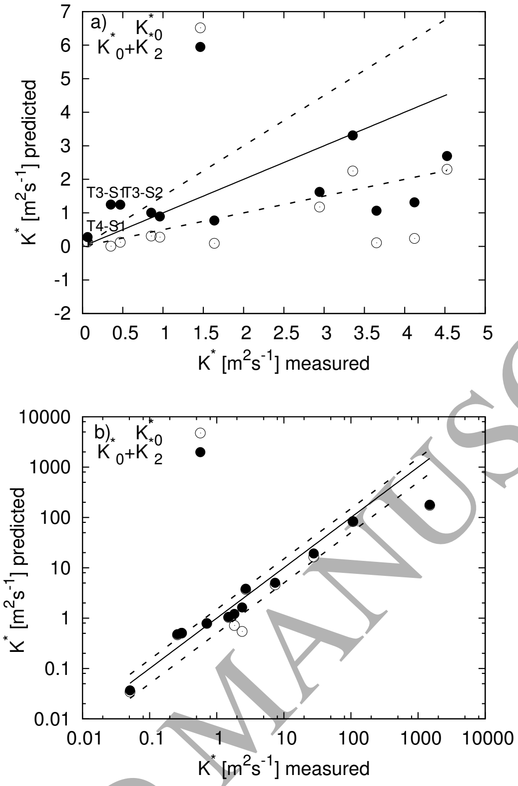

Figure 9: Comparison between the dispersion coefficients predicted by equations (31), (33) and those estimated from the tracer test carried out in meandering rivers: a) Copper River b.g. and Powell River; b) Copper b.g., Powell, Green-Duwamish, Lesser Slave, Missouri, Miljacka, Queich, Sulzbach , Ohio, Red Cedar rivers and in the experimental flume of *Boxall and Guymer* (2007). The sources of data are reported in Table 2. The continuous line denotes the perfect agreement; the dashed lines corresponds to a ± 50 % error.

transverse velocity gradients which, in turn, tend to increase the longitudinal dispersion coefficient. On the contrary, the increased transverse mixing promoted by secondary currents e.g., (*Boxall et al.*, 2003) would lead to a reduction of longitudinal dispersion. This behavior is summarized in the analytical relation (61), obtained by considering a regular sequence of sine generated bends.

Bend effects are explicitly accounted for through the dependence on ν^2 while the characteristics of the flow field and the bottom topography affect the co-

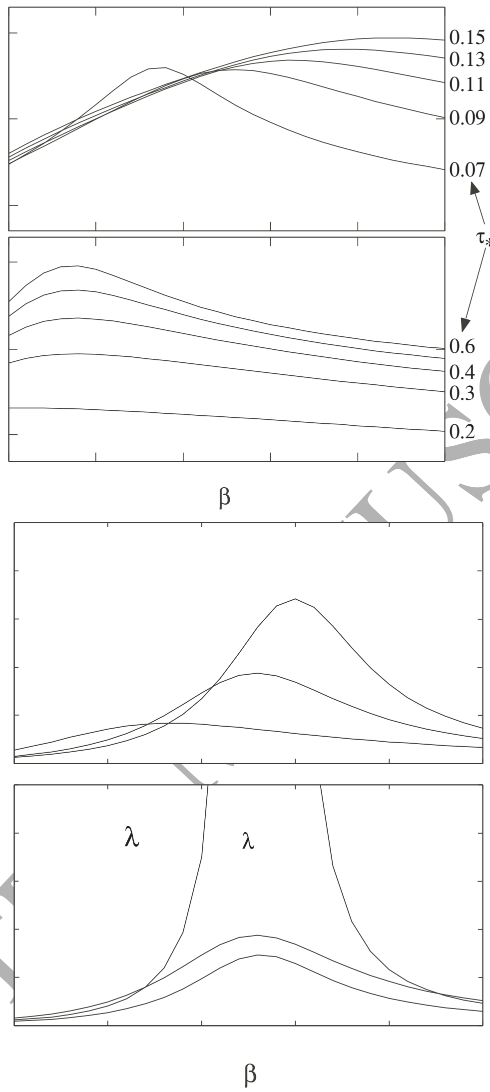

Figure 10: The theoretical values of bend averaged longitudinal dispersion coefficient $\mathcal{K}$ predicted by (61) are plotted versus the aspect ratio β for $\nu = 0.1$ and $k_{n0} = 0.225$. a) $\lambda = 0.1$, $d_{gr} = 0.01$, plane bed; . b) $\lambda = 0.1$, $d_{gr} = 0.001$, dune covered; c) $\tau_* = 0.09$; $\lambda = 0.1$, plane bed; d) $\tau_{*u} = 0.09$, $d_s = 0.01$, $\lambda = 0.1, 0.13, 0.16$.

efficients b_m. Moreover, as observed by *Fischer* (1969) and *Smith* (1983), the ratio γ of cross-sectional mixing timescale to longitudinal advection timescale, accounts for the frequency of alternating bends along the meandering reach. In the case of long enough bends, i.e such that γ is much smaller than 1, the term $(2\pi\gamma)^2$ at the denominator of (61) can be neglected with respect to M^4. On the contrary, if γ increases, K tends to decrease. This is the case of short bends, for which the changes in the flow field associated with alternating curves are too fast to allow cross-sectional mixing to eliminate concentration gradients.

Figure 10 shows two typical examples of the variations of K as a function of the aspect ratio β for either plane (Figure 10a) or dune-covered bed (Figure 10b). In both cases, for given values of the dimensionless parameters ν, d_{gr} and γ, the bend averaged longitudinal dispersion coefficient increases with the Shields parameter, τ_{*u}. On the other hand, for a given τ_{*u}, the values of K corresponding to quite different dimensionless grain sizes d_{gr} exhibit a relatively narrow range of variations, as shown in Figure 10c. Finally, Figure 10d demonstrates that K tends to increase significantly when approaching the resonant conditions (see, e.g., *Lanzoni and Seminara* (2006)). Nevertheless, it must be recalled that the meandering flow field in a neighborhood of the resonant state cannot be described by the linear model adopted here, but it would require a weakly nonlinear approach.

In general, the linearized treatment of the flow field set as the basis of the present theoretical framework holds for relatively wide bends (small ν), long enough meanders to ensure slow longitudinal variations of the flow field (small λ), small intensity of the centrifugally driven secondary flow, a condition met for small values of $\nu/(\beta\sqrt{c_{fu}})$, and small amplitude of bed perturbations with respect to the straight configuration (small $\nu\sqrt{\tau_{*u}/cfu}$ and $\lambda\beta\sqrt{\tau_{*u}}$) (*Bolla Pittaluga and Seminara*, 2011; *Frascati and Lanzoni*, 2013). These intrinsic limitation of the theory can partly explain the deviations of the predicted dispersion coefficients from the values estimated from tracer test data. Other physical processes however concur to the scatter of data. The bed configuration predicted by the considered hydro-morphodynamic model stems from the imposed flow discharge, corresponding to that actually observed during the tracer tests. Nevertheless, this discharge can differ from the formative discharge really producing the considered river bed configuration. The presence of regulation works and human activities (e.g., sediment mining, dredging) can modify the bed topography and, consequently, the structure of the flow field controlling shear flow dispersion. Finally, the presence of bedforms, width variations, islands, and dead zones all concur to a non-perfectly Fickian behavior, enhancing the rate of dispersion and causing the long tails usually observed in concentration-time curves. The Gaussian solution resulting from a Fickian approach to dispersion can then be used only to describe the upper portion of the concentration-time curves, as indicated by the tracer data plotted using Chatwin's transformation. Other approaches are needed to fit these curves, such as the transient storage models, that account for the effects of temporary entrapment and subsequent re-entrainment of pollutants (*Cheong and Seo*, 2003), the adoption of a fractional advection-dispersion equation (*Deng et al.*, 2004), or asymptotic treatment of one-dimensional solutions from an instantaneous point source (*Hunt*, 2006).

6. Conclusions

We set a physics-based theoretical framework to estimate the longitudinal dispersion coefficient on the basis of the hydro-morphodynamic modeling of the flow field and the bed topography that establish in alluvial rivers. The rational perturbative framework has been developed on the basis of a suitable scaling of the two-dimensional advection-diffusion equation, and by the introduction of a reference system moving with the contaminant cloud with a velocity that varies according to the cross sectional geometry. This framework provides a clear picture of the processes affecting the spreading of a contaminant in natural stream, that can be summarized as follows.

The longitudinal dispersion dynamics in alluvial rivers is controlled by velocity shear at the banks and secondary circulations driven by centrifugal and topographical effects. In particular, the helical flow associated to these circulations enhances relatively small and rapidly changing velocity and concentration gradients, both in the transverse and in the longitudinal directions, which in general lead to an increase of the longitudinal dispersion coefficient. Nevertheless, the planform shapes of meandering channels are usually characterized by relatively small values of the curvature ratio ν, implying that the increased transverse mixing, also promoted by secondary flows, affects the concentration distribution only at higher orders of approximation.

Another consequence of the small values typically attained by ν is the possibility to separate the contribution to shear flow dispersion provided by near bank velocity gradients associated to the unperturbed straight configuration (equation (31)) from that induced by streamline curvatures and by the alternating sequence of bars and pools which establishes in the perturbed meandering configuration (equation (33)). The former contribution can be accounted for analytically for gently sloping channel banks.

The longitudinal dispersion coefficient, averaged over the meander length in order to deal with longitudinal variations of the flow field, depends on the relevant bulk hydrodynamic and morphologic dimensionless parameters, β, d_{gr}, τ_{*u}, λ, ν and γ. The latter parameter, accounting for the ability of cross-sectional mixing to adapt to along-channel flow changes, could lead to a reduction of the longitudinal dispersion coefficient in the presence of a sequence of relatively short bends (equation (61)).

The comparison with field data obtained from tracer tests indicates that the proposed approach provides robust estimates of the reach averaged longitudinal dispersion coefficient. The residual scatter can be partly explained by the linearized character of the hydro-morphodynamic model used to estimate K^*. Flow nonlinearities, enhancing both transverse mixing and shear flow dispersion, induce opposite effects on longitudinal dispersion. Other possible causes of the departures between predicted and estimated coefficients are associated with the not entirely Fickian behavior of the dispersion process, whereby the concentration-time curves decay more slowly than if they were Gaussian.

Appendix A. Cross-sectional distribution of a uniform turbulent flow in a straight channel

Let us consider the longitudinal momentum equation averaged over the turbulence, written terms of the local curvilinear orthogonal coordinate system (s^*, σ^*, ζ^*) (*Lanzoni and D'Alpaos*, 2015):

$$\frac{\partial u^*}{\partial t^*} + u^* \frac{\partial u^*}{\partial s^*} + \frac{v^*}{h_\sigma} \frac{\partial u^*}{\partial \sigma^*} + w^* \frac{\partial u^*}{\partial \zeta^*} = -g \frac{\partial H^*}{\partial s^*} + \frac{1}{\rho\, h_\sigma} \left[\frac{\partial (h_\sigma T^*_{ss})}{\partial s^*} + \frac{\partial T^*_{\sigma s}}{\partial \sigma^*} + \frac{\partial (h_\sigma T^*_{\zeta s})}{\partial \zeta^*} \right] - \frac{v^2 + T_{\sigma\sigma}/\rho}{h_\sigma} \frac{\partial h_\sigma}{\partial s^*} \quad \text{(A.1)}$$

where h_σ is the metric coefficient associated with the curvilinear transverse coordinate σ, u^*, v^*, w^* are the components of the velocities along the three coordinate axes, H^* is the elevation of the water surface with respect to an horizontal reference plane, g is the gravitational constant, ρ is the water density and T^*_{ss},$T^*_{\sigma s}$,$T^*_{\zeta s}$, $T^*_{\sigma\sigma}$ are components of the turbulent Reynolds stress tensor. In the case of uniform flow conditions, as those occurring in a straight channel with a compact cross section (Figure 1c), the relevant variables do not vary in time and along the main flow direction s^*.

Expressing the components $T_{\sigma s}$ and $T_{\zeta s}$ of the Reynolds stress tensor through the Boussinesq eddy-viscosity approximation:

$$T_{\sigma s} = \rho \frac{\nu^*_T}{h_\sigma} \frac{\partial u^*}{\partial \sigma^*} \qquad T_{\zeta s} = \rho\, \nu^*_T \frac{\partial u^*}{\partial \zeta^*} \quad \text{(A.2)}$$

equation (A.1) simplifies to:

$$S\, h_\sigma\, g + \frac{\partial}{\partial \sigma^*} \left(\frac{\nu^*_T}{h_\sigma} \frac{\partial u^*}{\partial \sigma^*} \right) + \frac{\partial}{\partial \zeta^*} \left(\nu^*_T h_\sigma \frac{\partial u^*}{\partial \zeta^*} \right) = 0, \quad \text{(A.3)}$$

where $S = -\partial H^* / \partial s^*$ is the longitudinal water surface slope that, under uniform flow conditions, coincides with the bed slope and the energy slope, and ν^*_T is the turbulent eddy viscosity.

Under the assumption of a constant vertical distribution of the ν_T^*, the longitudinal slip-velocity at the bottom must satisfy the following condition:

$$u^*|_{\zeta^*=0} = u_f^* \left[2 + 2.5\, ln \left(\frac{D_z^*}{d_{gr}^*}\right)\right] \tag{A.4}$$

where $u_f^* = (gD_0^* S)^{1/2}$ is the local value of the friction velocity. In addition, the shear stress must vanish at the water surface and take the value ρu_f^{*2} at the bed, namely:

$$\left[\nu_T^* \left(\frac{\partial u^*}{\partial \zeta^*} - \frac{1}{h_\sigma^2}\frac{\partial D_z^*}{\partial p^*}\frac{\partial u^*}{\partial p^*}\right)\right]_{\zeta^*=D_z^*} = 0, \qquad \left[\nu_T^* \frac{\partial u^*}{\partial \zeta^*}\right]_{\zeta^*=0} = u_f^{*2} \tag{A.5}$$

In terms of the dimensionless variables (42) and (43), the problem described by equations (A.3), (A.4) and (A.5) becomes:

$$D_z^{-2}\frac{\partial}{\partial \zeta}\left[h_\sigma \nu_T \frac{\partial u}{\partial \zeta}\right] + \delta^2 \left(\frac{\partial}{\partial \sigma} - \zeta F_1 \frac{\partial}{\partial \zeta}\right)\left[\frac{\nu_T}{h_\sigma}\left(\frac{\partial}{\partial \sigma} - \zeta F_1 \frac{\partial}{\partial \zeta}\right) u\right] + h_\sigma = 0 \tag{A.6}$$

$$u|_{\zeta=0} = u_f \left[2 + 2.5\, ln \left(\frac{D_z}{d_{gr}}\right)\right] \tag{A.7}$$

$$\left[\nu_T \left(\frac{1}{D_0}\frac{\partial u}{\partial \zeta} - \frac{\delta^2}{h_\sigma}\frac{\partial u}{\partial \sigma}\right)\right]_{\zeta=1} = 0, \qquad \left[\frac{\nu_T}{D_z}\frac{\partial u}{\partial z}\right]_{\zeta=0} = u_f^2 \tag{A.8}$$

The solution of this problem is obtained by expanding $u(\zeta, \sigma)$ and $u_f(\sigma)$ in terms of the mall parameter δ:

$$\left(u, u_f\right) = \left(u_0, u_{f0}\right) + \delta^2 \left(u_1, u_{f_1}\right) + \mathcal{O}(\delta^4). \tag{A.9}$$

Substituting this expansion into equations (46), (A.7), (49), and collecting the terms with the same power of δ^2, we obtain a sequence of ordinary differential problems that can be readily solved in closed form. After some algebra we find:

- $O(\delta^0)$

$$u_0(\zeta, \sigma) = \left(-\frac{13\,\zeta^2}{2} + 13\,\zeta + 2 + \frac{5}{2}\ln\frac{D_0}{d_{gr}}\right)\sqrt{D_0} \tag{A.10}$$

$$u_{f_0}(\sigma) = \sqrt{D_0} \tag{A.11}$$

930 • $O(\delta^2)$

$$\begin{aligned} u_1(\zeta,\sigma) &= \sqrt{D_0}\Bigg\{\Bigg[\Big(\frac{45}{8}\ \ln(\frac{D_0}{d_{gr}})+\frac{7}{2}+\frac{25}{16}\ \ln(\frac{D_0}{d_{gr}})^2\Big)\frac{1}{13}+ \\ &\Big(-\frac{7}{8}-\frac{5}{16}\ \ln(\frac{D_0}{d_{gr}})\Big)\,\zeta^2+\Big(\frac{7}{4}+\frac{5}{8}\ \ln(\frac{D_0}{d_{gr}})\Big)\,\zeta+ \\ &\frac{5}{8}\ \ln(\frac{D_0}{d_{gr}})+\frac{1}{2}+13\Big(\frac{\zeta}{4}-\frac{\zeta^4}{16}+\frac{\zeta^3}{4}-\frac{3\,\zeta^2}{8}\Big)\Bigg] \\ &D_0\,\frac{\partial^2 D_0}{\partial\sigma^2}+\Bigg[\Big(\frac{205}{16}\ \ln(\frac{D_0}{d_{gr}})+\frac{33}{4}+\frac{25}{8}\ \ln(\frac{D_0}{d_{gr}})^2\Big)\frac{1}{13}- \\ &\frac{5\,\zeta^2}{16}+\Big(\frac{33}{8}+\frac{5}{4}\ \ln(\frac{D_0}{d_{gr}})\Big)\zeta+\frac{7}{4}+\frac{5}{8}\ \ln(\frac{D_0}{d_{gr}})+ \\ &13\Big(-\frac{\zeta^2}{8}-\frac{\zeta^4}{16}+\frac{\zeta}{4}\Big)\Bigg]\left(\frac{\partial D_0}{\partial\sigma}\right)^2\Bigg\} \end{aligned} \tag{A.12}$$

$$u_{f_1}(\sigma) = \frac{\sqrt{D_0}}{13}\left[\left(5+\frac{5}{8}\ \ln\frac{D_0}{d_{gr}}\right)D_0\,\frac{\partial^2 D_0}{\partial\sigma^2}+\left(\frac{59}{8}+\frac{5}{4}\ \ln\frac{D_0}{d_{gr}}\right)\left(\frac{\partial D_0}{\partial\sigma}\right)^2\right] \tag{A.13}$$

931 It is worthwhile to note that, at the leading order of approximation, the
932 friction velocity is proportional to the square root of the local flow depth (equa-
933 tion (A.11)), as it occurs under uniform flow conditions, while the first order
934 correction (equation (A.13)) quantifies the effects due to the cross slope and
935 curvature of the section bed profile.

936 The local value of the depth-averaged longitudinal velocity $U_0(\sigma) = U_{00}(\sigma)+$
937 $\delta^2 U_{01}(\sigma)$ is then determined by integrating u_0 and u_1 along the normal ζ. It
938 results:

$$U_{00} = \frac{u^*_{fu}}{U^*_u}\Big(\frac{19}{3}+2.5ln\frac{D_0}{d_{gr}}\Big)\sqrt{D_0} \tag{A.14}$$

$$\begin{aligned} U_{01} = \frac{u^*_{fu}}{U^*_u}\sqrt{D_0}\Bigg\{&\Big[\frac{781}{390}+\frac{395}{312}ln(\frac{D_0}{d_{gr}})+\frac{25}{208}ln^2(\frac{D_0}{d_{gr}})\Big]D_0 D_{0,\sigma\sigma} \\ &+\Big[\frac{17437}{3120}+\frac{465}{208}ln(\frac{D_0}{d_{gr}})+\frac{25}{104}ln^2(\frac{D_0}{d_{gr}})\Big]D_{0,\sigma}^{\,2}\Bigg\}+ \\ +\frac{u^*_{fu}}{U^*_u}\frac{\sqrt{D_0}}{2}\Bigg\{&\Big[\frac{5}{2}+\frac{5}{4}ln(\frac{D_0}{d_{gr}})D_{0,\sigma}\Big]+\Big[\frac{1}{D_0}\int_0^\sigma D_{0,\sigma}^{\,2}\,d\sigma-D_{0,\sigma}\Big]\Bigg\} \end{aligned}$$

Finally, we convert the coordinates σ to the corresponding Cartesian coordinates n by observing that:

$$n(\sigma) = \frac{1}{\beta\delta}\int_0^\sigma \sqrt{1-\left(\delta\frac{\partial D_0}{\partial \sigma'}\right)^2}\,d\sigma' = \frac{1}{\beta\delta}\left[\sigma - \frac{\delta^2}{2}\int_0^\sigma \left(\frac{\partial D_0}{\partial \sigma'}\right)^2 d\sigma' + \mathcal{O}(\delta^4)\right] \tag{A.15}$$

941 **Notations**

$A^*[m^2]$	local cross sectional area.
$A_u^*[m^2]$	mean value of the cross sectional area in the reach.
$B^*[m]$	free surface half width of the channel.
$B_c^*[m]$	half width of the central channel region.
$C[/]$	cross sectionally averaged concentration
$c[/]$	depth averaged concentration
$c_{fu}[/]$	friction coefficient
$\mathcal{C}[m^{-1}]]$	channel curvature
$D^*[m]$	local flow depth.
$D_c^*[m]$	flow depth of the central region of the channel.
$D_u^*[m]$	cross-sectionally averaged flow depth.
$D_z^*[m]$	flow depth measured normally to the bed.
$d_{gr}^*[m]$	grain size.
$d_r[m]$	discrepancy ratio.
$e_t^*[m^2/s]$	depth averaged eddy diffusity
$g[m/s^2]$	gravitational acceleration.
$H^*[m]$	elevation of the water surface with respect to an horizontal reference plane (942)
$H_u^*[m^{1.5}$	cross sectional average of $D^{*1.5}$
$(h_s, h_\sigma)[/]$	metric coefficients.
$K^*[m^2/s]$	mean value of the longitudinal dispersion coefficient in the reach.
$K_u^*[m^2/s]$	dispersion coefficient scale.
$k_{nu}^*[m^2/s]$	transversal mixing coefficient for a straight channel.
$(k_s^*, k_n^*)[m^2/s]$	longitudinal and transversal mixing coefficient.
$k_t^*[m^2/s]$	transverse dispersion coefficient.
$L^*[m]$	average intrinsic meander length.
$L_c^*[m]$	contaminant cloud length
$n^*[m]$	horizontal coordinate normal to s^*.
$P_0^*[m]$	wetted perimeter of each bank region of the channel.
$Q^*[m^3/s]$	flow discharge.
$R_0^*[m]$	twice the minimum value of the radius of curvature.
$r^*[m]$	local radius of curvature.
$S[/]$	longitudinal channel slope.
$s^*[m]$	longitudinal curvilinear coordinate coinciding with the channel axis.

$T_0^*[s]$	longitudinal dispersion time-scale.
$T_1^*[s]$	differential advection time-scale.
$T_2^*[s]$	transverse mixing time-scale.
$t^*[s]$	time.
$U^*[m/s]$	depth averaged longitudinal velocity.
$U_u^*[m/s]$	mean value of the cross sectionally averaged longitudinal velocity in the reach.
$u^*[m/s]$	longitudinal component of the velocity.
$u_f^*[m/s]$	local friction velocity.
$u_{fc}^*[m/s]$	scale for the friction velocity in the central region of the channel.
$u_{fu}^*[m/s]$	scale for the friction velocity under uniform flow conditions.
$u_{f0}, u_{f1}[/]$	leading and first order dimensionless friction velocity.
$V^*[m/s]$	depth averaged transverse component of velocity.
$z^*[m]$	upward directed axis.
$\beta[/]$	half free surface width to uniform depth ratio.
$\beta_c[/]$	half central region width to uniform depth ratio.
$\beta_f[/]$	cross section shape parameter measuring the steepness of the bank.
$\gamma[/]$	relative importance of transverse mixing and nonuniform trasport
$\Delta[/]$	immersed relative sediment density
$\delta[/]$	relative variation rate of the cross section in the transverse direction.
$\epsilon_n^*[m^2/s]$	transverse mixing coefficient contribution due to dispersion.
$\lambda[/]$	dimensionless meander wave number
$\zeta^*[m]$	coordinate normal to the bed.
$\xi^*[m]$	pseudo-lagrangian coordinate
$\lambda[m]$	
$\nu[/]$	curvature ratio
$\nu_T^*[m^2/s]$	turbulent viscosity.
$\rho[kg/m^3]$	water density.
$\rho_s[kg/m^3]$	sediment density.
$\sigma^*[m]$	transverse curvilinear coordinate.
φ	angle that the vertical forms with the normal to the bed

References

Alizadeh, M. J., Shahheydari, H., Kavianpour, M. R., Shamloo, H. and Barati, R.,(2017), Prediction of longitudinal dispersion coefficient in natural rivers using a cluster-based Bayesian network, *Environ. Earth. Sci.*, 76:86, doi: 10.1007/s12665-016-6379-6.

Bear, T., and P. C. Young (1983), Longitudinal dispersion in natural streams, *J. Environ. Eng.*, 109(5), 1049-1067.

Beltaos, S., and T. J. Day (1978), A field study of longitudinal dispersion, *Can. J. Civ. Eng.*, 5, 572-585.

Bencala, K. E., and R. A. Walters (1983), Simulation of solute transport in a mountain pool-and-riffle stream: A transient storage model, *Water Resour. Res.*, 19(3), 718-724.

Blondeaux, P., and G. Seminara (1985). A unified bar-bend theory of river meanders, *J. Fluid Mech.*, 157, 449-470.

Bolla Pittaluga, M., and G. Seminara (2011), Nonlinearity and unsteadiness in rivermeandering:Areview of progress in theory and modelling, *Earth Surf. Processes Landforms*, 36(1), 20-38, doi:10.1002/esp.2089.

Bogoni, M., Putti, M., and Lanzoni, S. (2017), Modeling meander morphodynamics over self-formed heterogeneous floodplains, *Water Resources Research*, doi: 10.1002/2017WR020726.

Botter G., and A. Rinaldo (2003), A Scale effect on geomorphologic and kinematic dispersion, *Water Resour. Res.*, 39(10).

Boxall, J.B., and I. Guymer (2007), Longitudinal mixing in meandering channels: New experimental data set and verification of a predictive technique, *Water Research*, 41, 341-354.

Boxall, J.B., I. Guymer, and A. Marion (2003), Transverse mixing in sinuous natural open channel flows, *Journal of Hydraulic Research*, 41, 153-165.

Chatwin, P.C. (1980), Presentation of longitudinal dispersion data, *J. Hydraul. Proc. ASCE*, 106, 71-83.

Chatwin, P.C., and M. Allen (1985), Mathematical models of dispersion in rivers and estuaries, *Ann. Rev. Fluid Mech.*, 17, 119-149.

Cheong, T. S., and I. W. Seo, (2003) Parameter estimation of the transient storage model by a routing method for river mixing processes, *Water Resour. Res.*, 39(4), 1074, doi:10.1029/2001WR000676.

Czernuszenko W., P. M. Rowinski and A. Sukhodolov, (1998), Experimental and numerical validation of the dead-zone model for longitudinal dispersion in rivers, *Journal of Hydraulic Research*, 36 (2), 269-280.

Deng, Z.Q., V. P. Singh and L. Bengtsson (2004), Numerical Solution of Fractional Advection-Dispersion Equation, *J. Hydr. Eng., ASCE*, 130(5), 422-431.

Deng, Z.Q., L. Bengtsson, V. P. Singh and D. D. Adrian (2002), Longitudinal dispersion coefficient in single-channel streams, *J. Hydr. Eng., ASCE*, 128(10), 901-916.

Deng Z.Q., V.P. Slingh, and L. Bengtsson (2001), Longitudinal dispersion coefficient in straight rivers, *J. Hydr. Eng.*, 10.1061/(ASCE)0733-9429(2001)127:11(919), 919-927.

Disley, T., Gharabaghi B., Mahboubi A., McBean E. (2015), Predictive equation for longitudinal dispersion coefficient, *Hydrol. Process*, 29:161-172.

Dobran, B.H. (1982), Dispersion in montainous natural streams. *J. Environ. Eng. Div., ASCE*, 108(EE3), 502-514.

Eke, E. C., G. Parker, and Y. Shimizu (2014), Numerical modeling of erosional and depositional bank processes in migrating river bends with self-formed width: morphodynamics of barp ush and bank pull, *J. Geophys. Res. Earth Surf.*.

Engelund F. (1974), Flow and bed topography in channels bends, *J. Hydraul. Div. ASCE*, 100(HY11), 1631-1648.

Etamad-Shahidi Frascati A., and S. Lanzoni (2013), Predicting longititudinal dispersion coefficient in natural streams using M5' model tree, *Journal Hydraul Eng.*., 138(6): 542-554.

Fischer, H. B. (1967), The mechanics of dispersion in natural streams, *J. of Hydraul. Div., ASCE*, 93(HY6), 187-216.

Fischer, H. B. (1968), Methods for predicting dispersion coefficients in natural streams, with application to lower reaches of the Green and Duwamish Rivers, Washington, U.S. *Geol. Survey Prof. Pap.* 582-A, 27 pp.

Fischer, H. B. (1969), The effects of bends on dispersion in streams, *Water Resour. Res*, 5, 496-506.

Fischer, H. B. (1973), Longitudinal dispersion and turbulent mixing in open channel flows, *Annual Review of Fluid Mechanics*, 5, 59-78.

Fischer, H. B., E. J. List, R. C. Y. Koh, J. Imberger, and N. H. Brooks (1979), *Mixing in Inland and Coastal Waters.*, Academic Press, New York.

Frascati A., and S. Lanzoni (2013), A mathematical model for meandering rivers with varying width, *Journal of Geophysical Res., Earth Surf.*, 118, 1641-1657, doi: 10.1002/jgrf.20084.

Frascati A., and S. Lanzoni (2009), Morphodynamic regime and long-term evolution of meandering rivers, *Journal of Geophysical Res., Earth Surf.*, 114, F02002, doi:10.1029/2008JF001101.

Frascati, A., and S. Lanzoni (2010), Long-term river meandering as a part of chaotic dynamics? A contribution from mathematical modelling, *Earth Surf. Process. Landforms*, 35(7), 791-802.

Godfrey R. G., and B.J. Frederick, (1970), Stream dispersion at selected sites, *U.S. Geol. Surv. Prof.Paper*, *433-K*, Washington D.C..

Guymer, I. (1998), Longitudinal dispersion in sinuous channel with changes in shape, *J. Hydraul. Eng., ASCE*, 124(1), 33-40.

Hey, R. D., and C. R. Thorne (1986), Stable channels with mobile gravel beds. *J. Hydraul. Eng., ASCE* 112(8), 671-689.

Howard, A. D. (1992), Modelling channel migration and floodplain sedimentation in meandering streams, in *Lowland Floodplain Rivers: Geomorphological Perspectives*, edited by Carling, P. and Petts, G.E., pp. 1-41, John Wiley & Sons Ltd.

Hunt, B. (2005), Asymptotic solutions for one-dimensional dispersion in rivers, *Journal of Hydraulic Engineering*, 132(1), doi: 10.1061/(ASCE)0733-9429(2006)132:1(87).

Iwasa, Y., and S. Aya (1991), Predicting longitudinal dispersion coefficient in open-channel flows. *Proc. Int. Symp. on Environ. Hydr., Hong Kong*, 505-510.

Kashefipour, S. M., and R. A. Falconer (2002), Longitudinal dispersion coefficient in natural channels, *Water Research* 36, 1596-1608.

Lanzoni, S., and A. D'Alpaos (2015), On funneling of tidal channels, *J. Geophys. Res. Earth Surf.*, 120, doi:10.1002/2014JF003203.

Lanzoni, S., and G. Seminara (2006), On the nature of meander instability, J. Geophys. Res., 111, F04006, doi:10.1029/2005JF000416.

Lees, M. J., L. A. Camacho, and S. Chapra (2000), On the relationship of transient storage and aggregated dead zone models of longitudinal transport in streams, *Water Resour. Res.*, 36(1), 213-224.

Leopold, L.B., M. G. Wolman, and J. P. Miller (1964), *Fluvial Processes in Geomorphology*, Freeman, New York.

Li, X., Liu H., Yin M., (2013), Differential evolution for prediction of longitudinal dispersion coefficients in natural streams. *Water Resour. Manag.*, 27:5245-5260.

Liu, H. (1977), Predicting dispersion coefficient of streams, *J. Envir. Eng. Div., ASCE*, 103(1), 59-69.

Marani, M., S. Lanzoni, D. Zandolin, G. Seminara, and A. Rinaldo (2002), Tidal meanders, *Water Resour. Res., ASCE*, 38(11), 1225, doi:10.1029/2001WR000404.

Morse, P. M., and Feshbach, H. (1953), *Methods of Theoretical Physics*, Pergamon, New York.

McQuivey, R. S. and Keefer, T. N. (1974), Simple method for predicting dispersion in rivers. *J. Envir. Engrg. Div.* 100(4), 977-1011.

Nayfeh, A. H. (1973), *Perturbation Methods*, pp. 1-425, John Wiley, New York.

Noori R., B. Ghiasi, H. Sheikhian and J. F. Adamowski (2017), Estimation of the dispersion coefficient in natural rivers using a granular computing model, *J. Hydraul. Eng.* 143(5): 04017001-1-12.

Nordin, C. F., and G. V. Sabol (1974), Empirical data on longitudinal dispersion in rivers. *U.S. Geol. Surv. Water Res. Invest.* 20-74, Washington, D.C.

Noss C. and A. Lorke, (2016), Roughness, resistance and dispersion: relationships in small streams, *Water Resour. Res.* 52: 2802-2821. doi:10.1002/2015WR017449.

Parker, G. (2004), 1D Sediment Transport Morphodynamics with Applications to Rivers and Turbidity Currents, *http://cee.uiuc.edu/people/parkerg/morphodynamics e- book.htm.*

Revelli R., and L. Ridolfi (2002), Influence of suspended sediment on the transport processes of nonlinear reactive substances in turbulent streams, *J. Fluid Mech.*, 472, 7-331.

Rinaldo A., A. Marani and R. Rigon (1991), Geomorphological dispersion, *Water Resour. Res.*, 27 (4), 513-525.

Rutherford, J. C. (1994), *River Mixing*, John Wiley, New York.

Sahay R., and S. Dutta (2009), Prediction of longitudinal dispersion coefficient in natural rivers using genetic algorithm, *Hydr.Res.*, 40(6):544-552.

Sattar A.M., and B. Gharabaghi (2015), Gene-expression models for prediction of longitudinal dispersion coefficient in streams., *J Hydrol.*, 524:587-596.

Schnoor, J. L. (1996), *Environmental Modeling*, John Wiley, New York.

Seminara, G. (2006), Meanders, *Journal Fluid Mech.*, 554, 271-297, doi: 10.1017/S0022112006008925.

Smeithlov, B. B. (1990), Effect of channel sinuosity on river turbulent diffusion, *Yangtze River*, 21(11), 62.

Smith, R. (1983), Longitudinal dispersion coefficients for varying channels, *J. Fluid Mech.* 130, 299-314.

Seo I. W., and T. S. Cheong (1998), Predicting longitudinal dispersion coefficient in natural streams, *J. Hydr. Eng. ASCE* 124(1), 25-32.

Shucksmith, J. D., J. B. Boxall, and I. Guymer (2011), Determining longitudinal dispersion coefficients for submerged vegetated flow, Water Resour. Res., 47, W10516, doi:10.1029/2011WR010547. 1.

Shen C., J. Niu, E.J. Anderson and M. S. Phanikumar (2010), Estimating longitudinal dispersion in rivers using acoustic doppler current profilers, *Adv. Water Res.*, 33, 615-623. doi:10.1029/2011WR010547. 1.

Smith, R., (1983), Longitudinal dispersion coefficient for varying channels, J. Fluid Mech. 130, 299-314.

Taylor, G. I. (1954), The dispersion of matter in turbulent flow through a pipe, *Proc. Royal Soc. London, Ser. A*, 223, 446-468.

Tubino M., and M. Colombini (1992) Correnti uniformi a superficie libera e sezione lentamente variabile, *XXIII Convegno di Idraulica e Costruzioni Idrauliche*, D.375-D.386.

Wallis, S. G. (1994), Simulation of solute transport in open channel flow. In: *Mixing and transport in the environment*, edited by K. J. Beven, P. Chatwin, and J. Millbank, pp. 89-112, John Wiley, New York.

Wang Y. and W. Huai (2016), Estimationg the longitudinal dispersion coefficient in straight natural rivers *J. Hydraul. Eng.*, 142(11):04016048-1-11.

Yotsukura, N., H. B. Fischer, and W. W. Sayre (1970), Measurement of mixing characteristics of the Missouri River between Sioux City, Iowa, and Plattsmouth, Nebraska. *U.S. Geol. Surv. Prof. Paper* 1899-G, Washington, D.C.

Yotsukura, N. (1977), Derivation of solute-transport eqiations for a turbulent natural-channel flow, *J. Research U.S. Geol. Survey* 5 (3), 277-284.

Zeng Y., Huai W. (2014), Estimation of longitudinal dispersion coefficient in rivers, *J. Hydro Environ Res.* 8: 2-8.